Article

SOURCE DATA

TRANSPARENT PROCESS

BH3-in-groove dimerization initiates and helix 9 dimerization expands Bax pore assembly in membranes

Zhi Zhang[1], Sabareesh Subramaniam[2,†], Justin Kale[3,†], Chenyi Liao[4,†], Bo Huang[5,†], Hetal Brahmbhatt[3], Samson GF Condon[2], Suzanne M Lapolla[1], Franklin A Hays[1,6], Jingzhen Ding[1], Feng He[1], Xuejun C Zhang[5], Jianing Li[4], Alessandro Senes[2], David W Andrews[3] & Jialing Lin[1,6,*]

Abstract

Pro-apoptotic Bax induces mitochondrial outer membrane permeabilization (MOMP) by forming oligomers through a largely undefined process. Using site-specific disulfide crosslinking, compartment-specific chemical labeling, and mutational analysis, we found that activated integral membrane Bax proteins form a BH3-in-groove dimer interface on the MOM surface similar to that observed in crystals. However, after the α5 helix was released into the MOM, the remaining interface with α2, α3, and α4 helices was rearranged. Another dimer interface was formed inside the MOM by two intersected or parallel α9 helices. Combinations of these interfaces generated oligomers in the MOM. Oligomerization was initiated by BH3-in-groove dimerization, without which neither the other dimerizations nor MOMP occurred. In contrast, α9 dimerization occurred downstream and was required for release of large but not small proteins from mitochondria. Moreover, the release of large proteins was facilitated by α9 insertion into the MOM and localization to the pore rim. Therefore, the BH3-in-groove dimerization on the MOM nucleates the assembly of an oligomeric Bax pore that is enlarged by α9 dimerization at the rim.

Introduction

In most cells, Bax is a monomeric protein in the cytosol. During apoptosis initiation, Bax is activated and targeted to the mitochondrial outer membrane (MOM). The active Bax undergoes a series of conformational changes and eventually forms oligomeric pores in the MOM that release cytochrome c and other mitochondrial intermembrane space proteins to activate caspases and nucleases, thereby dismantling the cells (Borner & Andrews, 2014; Chi *et al*, 2014; Moldoveanu *et al*, 2014; Volkmann *et al*, 2014; Westphal *et al*, 2014b).

Previous studies revealed a multi-step process that transforms Bax from a dormant soluble protein to an active integral membrane protein. Bax cycles on and off membranes by a process called retro-translocation (Edlich *et al*, 2011; Schellenberg *et al*, 2013). The Bax is activated and bound to mitochondria by BH3-only proteins such as tBid (Lovell *et al*, 2008) or by previously activated Bax (Tan *et al*, 2006). The activated Bax partially embeds helices α5, α6, and α9 into the MOM as cysteines positioned in these helices become inaccessible to a membrane-impermeant sulfhydryl-specific modifying agent when Bax inserts into membranes (Annis *et al*, 2005; Westphal *et al*, 2014a). Inaccessibility was observed for Bax bound to the mitochondria isolated from etoposide-treated Myc-null cells where Bax did not oligomerize, and from Myc-expressing cells where Bax did oligomerize, suggesting that the helices are inserted into the MOM before oligomerization (Annis *et al*, 2005). Consistent with this model, residue inaccessibility was also observed before the tBid-induced oligomerization of Bax mutants that were constitutively bound to mitochondria due to a mutation in α9 (Westphal *et al*, 2014a). The α5 insertion was also supported by an increase of fluorescence of an environment-sensing fluorophore attached to the α5 of Bax after it was activated by membrane-bound tBid (Lovell

1 Department of Biochemistry and Molecular Biology, University of Oklahoma Health Sciences Center, Oklahoma City, OK, USA
2 Department of Biochemistry, University of Wisconsin-Madison, Madison, WI, USA
3 Biological Sciences, Sunnybrook Research Institute, Department of Biochemistry, University of Toronto, Toronto, ON, Canada
4 Department of Chemistry, University of Vermont, Burlington, VT, USA
5 Institute of Biophysics, Chinese Academy of Sciences, Beijing, China
6 Peggy and Charles Stephenson Cancer Center, University of Oklahoma Health Sciences Center, Oklahoma City, OK, USA
*Corresponding author. Tel: +1 405 271 2227, Ext. 61216; E-mail: jialing-lin@ouhsc.edu
†These authors contributed equally to this work

et al, 2008). Kinetic analysis of the fluorescence changes associated with α5 insertion and Bax oligomerization indicated that the insertion occurred earlier than the oligomerization. However, while the early chemical labeling study concluded that the α5, α6, and α9 are deeply inserted into the lipid bilayer, the later study concluded that the α5 and α6 are shallowly inserted into the cytosolic leaflet of the bilayer with some α5 residues buried in the cytosolic domain of Bax oligomer after Bax is activated by tBid. Therefore, a more rigorous topology survey is required to differentiate the models for the three membrane-embedded helices, and to ascertain the topology of the other regions, particularly the BH3 region and its binding groove, which are critical to Bax interaction and function (Bleicken *et al*, 2010; Zhang *et al*, 2010; Dewson *et al*, 2012).

The structure of the oligomeric Bax pore was largely unexplored until recently. Our photocrosslinking study revealed two interdependent interfaces in the Bax oligomer formed in detergent micelles (Zhang *et al*, 2010). A double electron–electron resonance (DEER) study of Bax oligomer formed in detergent micelle and liposomal membrane suggested an antiparallel helical dimer interface formed by α2-α3 region of neighboring Bax molecules in the oligomer (Bleicken *et al*, 2010). A disulfide-crosslinking study indicated that the antiparallel α2-α3 interface was extended to include α4 which binds to the other side of α2, and this interface together with a parallel α6 interface could generate Bax oligomers in the MOM (Dewson *et al*, 2012). Another disulfide-crosslinking study detected an α9 interface formed by a Bax mutant constitutively bound to mitochondria (Iyer *et al*, 2015). Whether wild-type Bax can form this α9 interface was unknown. Moreover, the contribution of all of these interfaces to the oligomeric pore assembly has not been assessed.

A crystallographic study revealed structures of three Bax complexes (Czabotar *et al*, 2013). The first is a domain-swapped dimer in which two Bax polypeptides lacking the C-terminal α9 helix (BaxΔα9) swap their α6-α8 helices, resulting in two globular units, each comprising α1-α5 helices from one monomer (the core domain), plus α6-α8 helices from the other monomer (the latch domain), that are bridged by two extended antiparallel α5-α6

helices. The second is the domain-swapped BaxΔα9 dimer with a BH3 peptide of tBid bound to each globular unit via a hydrophobic groove that is occupied by α9 in full-length Bax monomer (Suzuki *et al*, 2000). The third was formed by a GFP fusion protein containing Bax α2-α5 helices. A symmetric dimer interface exists in this complex, in which the BH3 region or α2 of one Bax fragment engages a groove in the other Bax fragment and vice versa, resulting in two reciprocal BH3-in-groove interfaces (Fig 1A).

Based on these crystal structures, the following model was proposed for Bax activation and oligomerization (Czabotar *et al*, 2013). Binding of a BH3-only protein to the hydrophobic groove of Bax after α9 is released from the groove and inserted into the MOM triggers the release of the latch domain from the core domain and the exposure of the BH3 region. The exposed BH3 region of one Bax replaces the BH3-only protein from the groove of other Bax and vice versa, resulting in a Bax homodimer with the BH3-in-groove interface that nucleates the oligomerization process. In addition, a hydrophobic patch consisting of aromatic residues from α4 to α5 that is located on one side of the BH3-in-groove dimer engages the MOM to promote MOMP (Fig 2A, top-left). However, these inferences were made based on the structure of a domain-swapped dimer that is acknowledged to be an off mechanism dead-end complex and the structures of Bax deletion mutants, some of them fused with GFP and all of them formed without membranes. Although the core–latch separation and the BH3-in-groove dimerization were confirmed recently by a DEER study that measured the intra- and intermolecular distances of tBid-activated liposome-bound Bax molecules with spin-labeled cysteines (Bleicken *et al*, 2014), the broad distance distributions implied that the Bax oligomer structure might be dynamic and flexible. Moreover, only three intramolecular distances were obtained from mitochondrion-bound Bax. Thus, it was uncertain whether the domain separation and dimerization actually occurred for the Bax at mitochondria.

Förster resonance energy transfer (FRET) was used to measure intramolecular distances within a Bax molecule and intermolecular distances between two Bax molecules in the cytosol or the mitochondria of live and apoptotic cells (Gahl *et al*, 2014). The

---

Figure 1. Activated Bax proteins integrate into the MOM and dimerize via a BH3-in-groove interface.

A   The crystal structure of the BH3-in-groove Bax homodimer (PDB entry 4BDU) is shown with one monomer colored gray and the other colored green, magenta, blue, and red for its α2, α3, α4, and α5 helices, respectively, as indicated. The residue pairs that were replaced with cysteine pairs in (B) are presented in stick form, and their β-carbon atoms linked by dashed lines with the distances ranging from 5.0 to 6.0 Å.

B   The *in vitro* synthesized [^{35}S]Met-labeled single-cysteine Bax proteins were activated and targeted to the mitochondria that were pretreated with NEM to block the sulfhydryls of mitochondrial proteins. The resulting mitochondria were isolated and oxidized by CuPhe for 30 min. NEM and EDTA were then added to stop the oxidation. For the "0 min" controls, NEM and EDTA were added before the addition of CuPhe. The resulting samples were analyzed by phosphorimaging after non-reducing or reducing SDS–PAGE (see Appendix Fig S2A).

C   Oxidized mitochondria with the radioactive single-cysteine Bax protein pair or double-cysteine Bax protein were prepared and analyzed as in (B).

D   Oxidized mitochondria with the radioactive single-cysteine Bax protein pair or double-cysteine Bax protein were prepared as in (B). After an aliquot was withdrawn as input, another aliquot was extracted by Na$_2$CO$_3$ (pH 11.5) and centrifuged through a sucrose cushion to separate the integral proteins in the membrane pellet from the soluble and peripheral proteins in the supernatant. The input, pellet, and supernatant were analyzed by non-reducing SDS–PAGE and phosphorimaging. In a parallel control experiment, the pellet and supernatant were analyzed by reducing SDS–PAGE and immunoblotting with an antibody specific to PDHE1α, a soluble mitochondrial matrix protein.

Data information: In (B–D), protein standards are indicated on the side of phosphor images or immunoblots by their molecular mass (M$_r$). Open circles indicate Bax monomers. Upward arrows indicate disulfide-linked dimers of the same single-cysteine Bax mutant (e.g., M79C), and downward arrows disulfide-linked dimers of two different single-cysteine Bax mutants (e.g., L59C + M79C) or of the same double-cysteine Bax mutant (L59C,M79C). Closed circles indicate the disulfide-linked heterodimer of Bax M79C and the BH3 peptide (with a cysteine at position 62). The number of independent replicates done for each Bax mutant in (B–C), n = 2 for C62+M79C, T56C, and R94C; 3 for L63C, L63C+A112C, A112C, K64C, K64C+M79C, and M99C; 4 for L59C+M79C, M79C, C62, C62+L76C, and T56C+R94C; 6 for L59C, and L76C; and 8 for L59C,M79C. For each Bax mutant and PDHE1α in (D), n = 2.

Source data are available online for this figure.

intramolecular distance from the donor dye-labeled α2 to the acceptor dye-labeled α7 was increased after Bax translocation from the cytosol to the mitochondria, consistent with the core–latch separation model. However, a significant decrease in FRET efficiency between the donor at α2 and the acceptor at α5 suggested a large conformational change within the core that separates the two
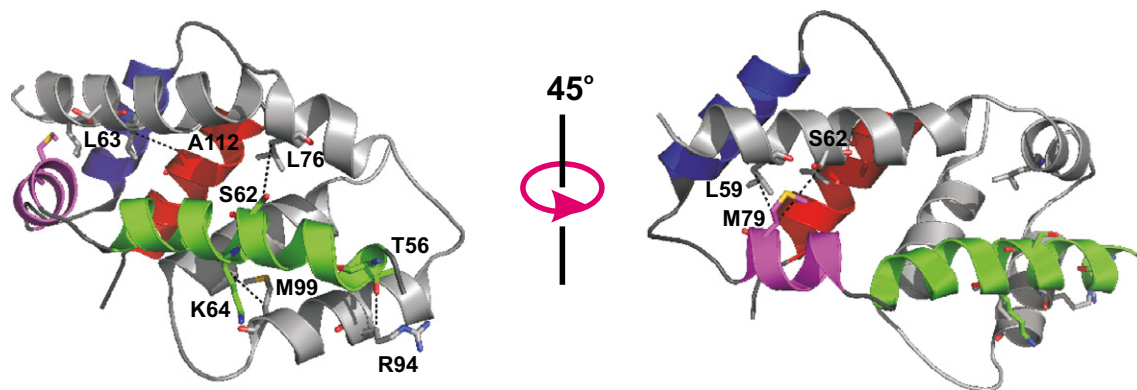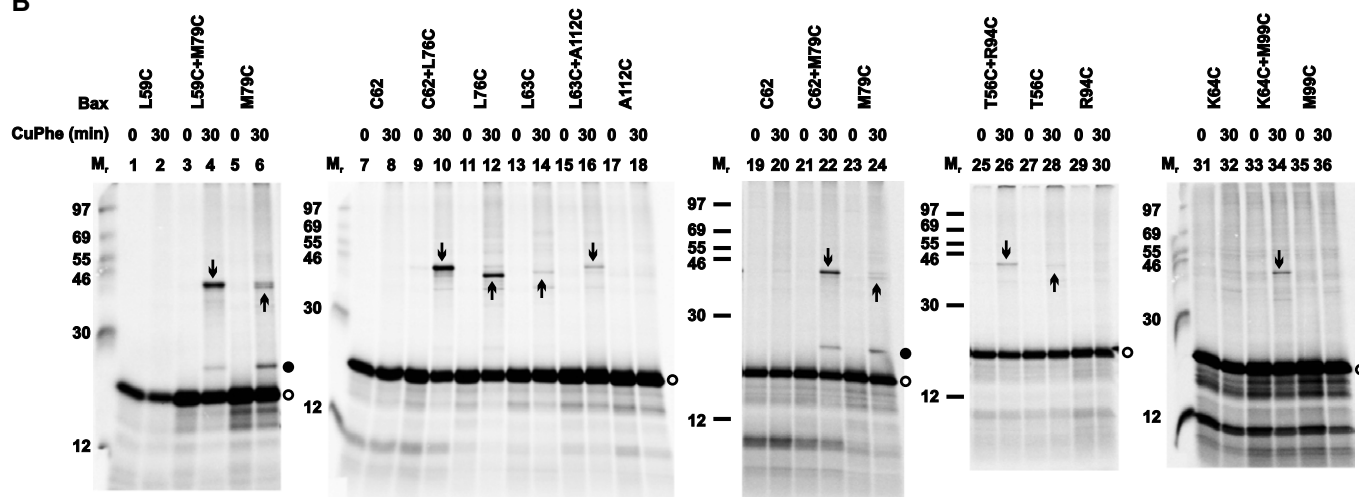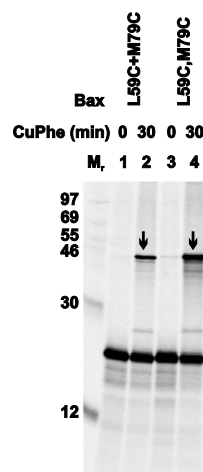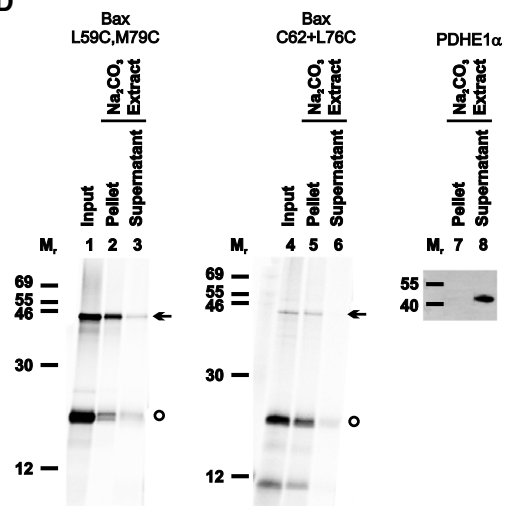

Figure 1.

Figure 2. The BH3 region and the groove are partially embedded in the MOM.

A   Top-left panel, structure of the BH3-in-groove dimer (PDB entry 4BDU) with the predicted MOM-engaging residues presented in stick form. Bottom-left panel, structure of the BH3-in-groove dimer with the predicted protein-buried residues presented in stick form. Top-right panel, structure of the BH3-in-groove dimer without helix α5 (modified from PDB entry 4BDU), and bottom-right panel, structure of α5 (extracted from the NMR structure of Bax monomer, PDB entry 1F16). In both structures in the right panels, the residues that are buried in the MOM or exposed to the aqueous milieu as the IASD-labeling data in (B–D) confirmed are presented in yellow or cyan stick form, respectively. In all panels, the color codes for the two monomers are the same as that in Fig 1A, and indicated.

B   The *in vitro* synthesized radioactive Bax proteins, each with a single cysteine positioned in helix α2, α3, α4, or α5, were activated and targeted to the mitochondria. The resulting mitochondria were isolated and treated with IASD in the absence or presence of CHAPS, urea, or both. After 30 min, the labeling reactions were stopped by mercaptoethanol. For the "0 min" controls, the samples were pretreated with mercaptoethanol before addition of IASD. The IASD-labeled radioactive Bax proteins were resolved from the unlabeled ones using either isoelectric focusing (IEF; as indicated) or gradient SDS–PAGE and detected by phosphorimaging. Triangles and arrows indicate the unlabeled and IASD-labeled Bax proteins, respectively. n = 3 for V111C, and K119C; 4 for W107C, and A117C; 2 for other mutants.

C, D   The phosphorimaging data for IASD labeling of Bax mutants in (B) and the similar data from the independent replicates were quantified to derive the membrane or protein burial indices as described and shown in Appendix Fig S3. The membrane burial indices were normalized by that of G179C in α9, a reference for the membrane-buried residues. The resulting relative membrane burial indices are shown in (C). The residues with the relative membrane burial index ≥40% of that of Gly[179] are considered as buried in the MOM. Similarly, the relative protein burial indices shown in (D) were obtained by using Y115C in α5 as a reference for the protein-buried residues. The residues with the relative protein burial index ≥40% of that of Tyr[115] are considered as buried in the protein or its complex.

Source data are available online for this figure.

helices further apart, inconsistent with the subtle distance changes between the two sites during a transition from the monomer NMR structure to the domain-swapped and the BH3-in-groove dimer crystal structures (Suzuki *et al*, 2000; Czabotar *et al*, 2013). In addition, the FRET distance between α9 and α2 indicated that α9 was distant from the canonical groove in the cytosolic Bax, thereby exposing the groove and BH3 region for potential homo- and hetero-interactions. After migrating to the mitochondria, while the intramolecular distance between α9 and α2 remained large and in accordance with the proposed core–latch separation, the intermolecular distance measured by the FRET between a donor-labeled α9 in one Bax molecule and an acceptor-labeled α9 in other Bax molecule was comparable with a homodimerization between the two α9 helices, in line with a model proposed in the DEER and crosslinking studies (Bleicken *et al*, 2014; Iyer *et al*, 2015). However, the DEER study proposed an antiparallel α9 dimer model, different from the parallel dimer model proposed by the other studies. Furthermore, intermolecular FRET measurements supported a Bax oligomer model in which in addition to the α9 dimer interface, α2 and α3 form the other dimer interface that unlike the crystallographic BH3-in-groove interface does not involve α5.

To further refine the mechanism of Bax activation and oligomerization, several important questions must be addressed. Does reciprocal binding of the BH3 region of one Bax to the groove of other Bax indeed occur at the MOM resulting in a BH3-in-groove dimer interface as revealed by crystallography? Does formation of the BH3-in-groove interface nucleate Bax oligomerization? For an oligomer to form, there must be additional dimer interfaces, but what regions of Bax are involved? In particular, does α9 form an additional interface, which together with the BH3-in-groove interface mediates Bax oligomerization? Are these dimer interfaces located above, on or in the MOM? If the BH3-in-groove dimer interface is located on the membrane surface with the hydrophobic patch engaging the membrane as the crystallography study proposed and the DEER and one chemical labeling study concluded (Czabotar *et al*, 2013; Bleicken *et al*, 2014; Westphal *et al*, 2014a), could that drive the hydrophobic patch, particularly the hydrophobic α5 helix, more deeply into the membrane as the other chemical labeling study suggested (Annis *et al*, 2005)? If the α5 inserts into the membrane and thereby separates from the rest of the BH3-in-groove dimer as the FRET study indicated (Gahl *et al*, 2014), would the remnant

interface rearrange to another conformation that is more stable? In other words, does the BH3-in-groove dimer represent a transient intermediate state? Most importantly, how do Bax oligomers form pores in the MOM? And how flexible is the pore structure? Accumulating evidence suggests that the pores are proteolipidic with some regions of Bax embedded into one leaflet of the bilayer to increase the membrane tension to a point that the bilayer would fuse to a highly curved monolayer, resulting in a toroidal pore with polar and charged lipid head groups lining the rim (Garcia-Saez, 2012). Other regions of Bax might localize to the rim to decrease the line tension, thereby stabilizing the lipidic pore. However, what are the Bax regions that induce, and that stabilize the lipidic pore? Finally, the size of Bax pore is tunable (Bleicken *et al*, 2013), but does higher order oligomerization expand the pore?

To answer these questions, we used disulfide crosslinking to map the dimer interfaces in the active mitochondrial Bax oligomer, and compartment-specific chemical labeling to determine the membrane topology. We built structural models and conducted molecular dynamics (MD) simulations to fit the experimental data, and generated mutations to test the functional relevance of the models. Based on these data and models, we propose a molecular scheme for how active Bax proteins are assembled into oligomers to induce and expand lipidic pores in the MOM.

Results

Bax mutants for interface and topology mapping are functional

Bax mutants with single, double, or triple cysteines located at specific positions were generated from a Bax cysteine-null mutant (Fig EV1A). The mutant proteins were synthesized by using a coupled *in vitro* transcription and translation (TNT) system, and their tBid-dependent MOMP activity was measured in an *in vitro* cytochrome c release assay (Ding *et al*, 2014) using Bax and Bak double deficient mitochondria (Bax$^{-/-}$/Bak$^{-/-}$ mitochondria) (Billen *et al*, 2008). Addition of both tBid protein and the wild-type (WT) Bax protein-producing TNT mixture resulted in a synergistic increase in cytochrome c released above the protein-independent background release (Fig EV1B, compare the open bars from "+Bax WT, +tBid" and "+Vector" samples). The releases above the background,
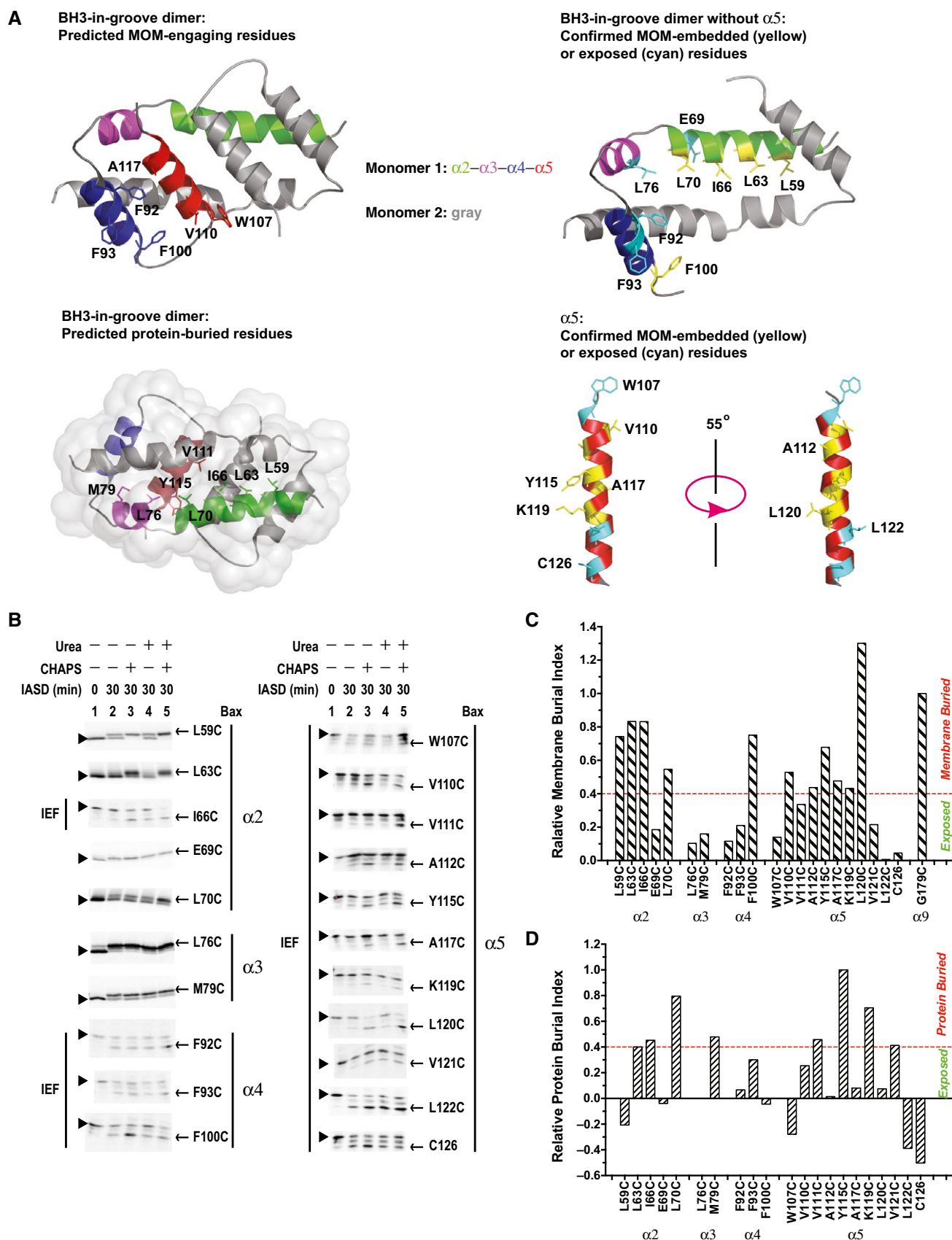
Figure 2.

indicated as the "corrected" releases (hatched bars) calculated from the "raw" releases (open bars) as described in the legend, showed the protein-dependent releases of cytochrome c by tBid (~20%), Bax (~0%), and both (~50%). With the background release common to these samples subtracted, the "corrected" data in Fig EV1C demonstrated that the cytochrome c release due to Bax alone is ~10% or lower for the wild-type Bax and all the mutants, except for L76C and V110C. These two mutants are "autoactive" as they released ~30–60% of cytochrome c in the absence of tBid. As expected, addition of tBid to the "non-autoactive" Bax mutants increased the release to ~30–60%, comparable to the wild-type Bax. Even though some of the mitochondria are somewhat leaky in our *in vitro* lysate-based system (Fig EV1B, "Mito-only" sample), the intact mitochondria still respond to the tBid and Bax proteins appropriately.

To relate this *in vitro* MOMP activity to apoptotic activity in live cells, we expressed the two single- and two double-cysteine mutants that were most frequently used in this study transiently as Venus fusion proteins in *bax/bak* double-knockout baby mouse kidney (*bax/bak* DKO BMK) cells (Fig EV2). We compared their intracellular location and apoptotic activity before and after staurosporine (STS) treatment to that of wild-type Bax and the cysteine-null mutant. Average Venus fluorescence per cell was measured and correlated to the protein expression. All mutant constructs were expressed at similar levels compared to Venus-WT Bax (Fig EV2A). Expression of Venus-WT Bax increased apoptosis compared to the Venus-only control, and the STS treatment further increased apoptosis (Fig EV2B). Consistent with the results from the *in vitro* MOMP assay, the cysteine-null (C0), the single-cysteine (A178C and A183C), and the double-cysteine (L59C,M79C and L59C,L76C) mutants significantly elevated apoptosis in response to STS like the wild-type protein. In addition, the intracellular localizations of these mutants and the Venus-WT Bax are similar, mostly in the cytoplasm but partially at the mitochondria in the untreated cells (Fig EV2C and D). The only exception is Venus-Bax L59C,L76C, which is mostly localized to the mitochondria. As expected, these intracellular localization data are in line with the mitochondrial binding data obtained *in vitro* (Appendix Fig S1, and below).

In addition, previous studies showed that the following Bax mutants, T56C, E69C, R94C, L122C, C126, I175C, V177C, A178C, G179C, and V180C, were active in *bax/bak* double-knockout mouse embryo fibroblast cells, inducing apoptosis after etoposide treatment like WT Bax (Dewson *et al*, 2012; Westphal *et al*, 2014a; Iyer *et al*, 2015). Thus, the cytochrome c release by these mutants *in vitro* (Fig EV1C) is consistent with their apoptotic activity in cells. Therefore, the Bax mutants used here to map the dimer interface and membrane topology are functionally similar to the wild-type protein, ensuring that structural information obtained from them is relevant to the functional MOM-bound Bax.

The BH3-in-groove dimer interface exists in the MOM-bound Bax complex

To determine whether the BH3-in-groove dimer interface observed in crystals exists in the MOM-bound Bax complex, we generated Bax mutants with single cysteines located throughout the BH3 region and the groove. Some of the cysteines are located in the known dimer interface and thus expected to form a disulfide-linked dimer (Fig 1A). Other cysteines are located farther away in the

dimer structure and thus not expected to form a disulfide. We synthesized the [^{35}S]Met-labeled Bax mutants in an *in vitro* translation system, activated them with a Bax BH3 peptide, and targeted them to the Bax$^{-/-}$/Bak$^{-/-}$ mitochondria. The mitochondria-bound proteins were separated from the soluble ones and oxidized with copper(II)(1,10-phenanthroline)$_3$ (CuPhe). The resulting radioactive proteins and the potential disulfide-linked protein complexes were analyzed using non-reducing SDS–PAGE and phosphorimaging. A radioactive product of an apparent molecular mass (M_r) close to that of a Bax homodimer (Fig 1B, indicated by downward arrow) was detected with each of the indicated single-cysteine Bax pairs predicted to form a disulfide-linked Bax homodimer according to the BH3-in-groove dimer structure (Fig 1A).

The following eight lines of evidence demonstrated that the products indicated by downward arrows in Fig 1B are the disulfide-linked dimers of the corresponding single-cysteine Bax pairs after they were activated and integrated into the MOM.

1   These products appeared on the non-reducing gel (Fig 1B) and disappeared on the reducing gel (Appendix Fig S2A) and were not formed by the cysteine-null Bax (C0) (Fig EV3A) or when NEM or EDTA was added to block the sulfhydryl and chelate the Cu^{2+}, respectively, before the addition of CuPhe to catalyze the oxidation (Fig 1B, CuPhe 0 versus 30 min). Therefore, they are disulfide-linked products generated from the oxidized single-cysteine Bax pairs.

2   Bax L59C, C62, R94C, M99C, or A112C did not form a disulfide-linked homodimer (Fig 1B, lane 2, 8, 30, 36, or 18). However, when they were paired with another Bax mutant, M79C, L76C, S56C, K64C, or L63C, respectively, a disulfide-linked dimer was formed (lane 4, 10, 26, 34, or 16, indicated by a downward arrow). Therefore, each of these single-cysteine Bax pairs formed a disulfide-linked heterodimer.

3   Although Bax L63C, L76C, or M79C formed a disulfide-linked homodimer (Fig 1B, lane 14, 12, or 24, indicated by upward arrow), a new disulfide-linked dimer of a slightly higher M_r was formed when they were paired with Bax A112C, C62, or C62, respectively (lane 16, 10, or 22, indicated by downward arrow), suggesting that the new dimer is a heterodimer formed by the respective single-cysteine Bax pair.

4   Bax T56C or M79C also formed a disulfide-linked homodimer (Fig 1B, lane 28 or 6, indicated by upward arrow), and the disulfide-linked dimer formed when they were paired with Bax R94C or L59C, respectively (lane 26 or 4, indicated by downward arrow), had a similar M_r as the corresponding homodimer. However, the yield of the dimer formed in the presence of the paired mutants was higher than that of the homodimer formed by the single mutant, suggesting that some of the dimers formed in the presence of the paired mutants are the disulfide-linked heterodimers. Consistent with this hypothesis, a disulfide-linked dimer was formed in a reaction containing ^{35}S-labeled Bax M79C and unlabeled but six-histidine (6H)-tagged Bax L59C, and detected by phosphorimaging in the Ni^{2+}-bound fraction (Fig EV3B, lane 2, indicated by arrow), demonstrating that the dimer contains both the ^{35}S-Bax and the 6H-Bax mutants. In a parallel reaction containing only the ^{35}S-Bax mutant, the dimer was not detected in the Ni^{2+}-bound fraction (lane 3). Therefore, the dimer detected in the reaction containing both the ^{35}S-Bax

and the 6H-Bax mutants must be the disulfide-linked heterodimer of these two mutants. A similar "epitope tagging" experiment to prove the disulfide linkage between T56C and R94C was unnecessary because this disulfide-linked heterodimer was detected before in mitochondria isolated from apoptotic cells expressing the two mutants with different tags (Dewson *et al*, 2012).

5   The yield of the disulfide-linked dimer formed by the double-cysteine mutant Bax L59C,M79C was doubled compared to that formed by the two corresponding single-cysteine mutants L59C and M79C when mixed together (Fig 1C, lane 4 versus 2, indicated by arrow). Therefore, this mutant was examined in more detail.

6   A disulfide-linked dimer of the double-cysteine mutant was not detected in the absence of the Bax$^{-/-}$Bak$^{-/-}$ mitochondria, the BH3 peptide, or both (Fig EV3C, lanes 1, 2, and 3 versus 4, indicated by arrow). Most of the Bax L59C,M79C monomer and the disulfide-linked dimer remained in the mitochondrial pellet fraction after Na$_2$CO$_3$ (pH 11.5) extraction as expected for integral membrane proteins (Fig 1D, lane 2 versus 3, indicated by open circle and arrow, respectively), whereas a soluble mitochondrial matrix protein, pyruvate dehydrogenase E1-alpha subunit (PDHE1α), was extracted to the supernatant fraction (lane 7 versus 8). Similar data were obtained for the single-cysteine Bax C62 and L76C pair after the Na$_2$CO$_3$ extraction (lane 5 versus 6).

7   In all the experiments above, Bax was activated by the Bax BH3 peptide that mostly stayed in the soluble fraction and hence would not interfere with the homodimerization of Bax proteins at the mitochondria via the same BH3-binding groove. To verify the results obtained from the BH3 peptide, we used tBid or caspase-cleaved Bid (cBid), a BH3 protein known to activate Bax in cells. Both tBid and cBid activations induced Bax homodimerization at the mitochondria as detected by the disulfide crosslinking of the L59C,M79C mutant, although the intensity of the homodimer band was less than that induced by the BH3 peptide (Fig EV3D, indicated by arrow), a result expected from the competition between Bax homo- and Bax-tBid hetero-dimerization.

8   The disulfide-linked homodimer of Bax L59C,M79C was clearly detected in the mitochondrial pellet fraction only after activation by cBid (Fig EV3E, indicated by arrow), consistent with the result from the BH3 peptide-activated Bax mutant (Fig EV3C). In the soluble supernatant fraction, a band of the same M_r as the Bax homodimer was detected in the CuPhe-induced disulfide-crosslinking samples (Fig EV3E, indicated by open triangle). However, because it was also formed before the CuPhe induction, it was not a disulfide-linked product, just like most of the other bands detected in these supernatant samples. Further, the specificity for where and when the Bax homodimer-specific disulfide linkage can form suggests that the introduction of cysteine into Bax by itself does not enhance the dimerization. Instead, our data indicate that disulfide linkage of these cysteine mutants can be used to probe the dimer formation by active Bax molecules at the mitochondria.

Together, these results demonstrate that Bax dimers, as detected by the disulfide crosslinking, were formed only after the Bax mutants were activated by the BH3 peptide or protein and inserted into the MOM. This result is consistent with reports suggesting that Bax oligomerization occurs after the protein inserts into membranes

(Annis *et al*, 2005; Lovell *et al*, 2008). Moreover, our data are consistent with a twofold symmetry of the BH3-in-groove structure for the core domain of Bax, further validating that the integral Bax proteins in the MOM form a symmetric dimer interface similar to that observed by crystallography.

The crystal structure of the Bax core dimer shows that two α5 helices are aligned in antiparallel forming the last part of the BH3-in-groove dimer interface (Czabotar *et al*, 2013). If the MOM-bound Bax proteins formed a dimer interface exactly like that in the crystal, cysteine substitution of Val^{111} in one Bax and Tyr^{115} in other Bax would generate a disulfide-linked dimer after the two Bax mutants were activated and integrated into the MOM. However, such a dimer was not detected (Fig EV3F), suggesting that the two α5 helices in the MOM-bound Bax dimer may not interact exactly like those in the crystal. To further probe the proximity of the α5 helices, we used BMH, a chemical crosslinker with a spacer of 13 Å between the two sulfhydryl-reactive maleimides, to crosslink the MOM-bound Bax mutants with single cysteine located in α5. Two W107C or Y115C monomers were crosslinked by BMH forming a homodimer (Fig EV3G). Similarly when the single cysteine was positioned in α2 in the I66C or L70C mutant, a BMH-crosslinked homodimer was also detected. Because the distance between the β-carbons of each of these residues in the BH3-in-groove dimer is from 8 to 18 Å (Fig EV3H), the cysteine replacements would be located within the range that can be linked by BMH, if one considers the flexibility of the BMH spacer and the cysteine side chain. The BMH crosslinking experiments thus revealed that the two α5 and the two α2 helices are in close proximity in the MOM-bound Bax dimer. Taken together with the disulfide-crosslinking data above, these chemical crosslinking results corroborate the existence of a BH3-in-groove interface in the active mitochondrial Bax complex, which is similar but not identical to the crystal structure of the Bax core dimer.

Helix α5 is embedded partially in the MOM, whereas helices α2, α3, and α4 are located on the surface

A hydrophobic patch was observed on one side of the BH3-in-groove dimer crystal that includes the aromatic residues from both α4 (Phe^{92}, Phe^{93}, and Phe^{100}) and α5 (Trp^{107}) (Fig 2A, top-left). If this hydrophobic patch engaged the MOM as proposed in the crystallographic study, it might lead to the integration of these helices into the MOM, particularly the more hydrophobic α5. To determine whether the hydrophobic patch is embedded in the membrane and the rest of the BH3-in-groove dimer structure is located on the surface, we used IASD, a membrane-impermeant sulfhydryl-specific labeling agent (Annis *et al*, 2005), to label Bax mutants with single cysteine positioned throughout the BH3-in-groove structure after they were activated by the BH3 peptide and targeted to Bax$^{-/-}$/Bak$^{-/-}$ mitochondria. In this procedure, surface-accessible cysteine residues are labeled by IASD directly; residues buried inside proteins are more labeled when the reactions include urea to loosen protein structures; and residues buried in the membrane-embedded protein domains are most efficiently labeled in the reactions containing both urea and the detergent CHAPS to unfold the protein and solubilize the membrane. The amino acid sequence surrounding the cysteine residue might also influence the labeling efficiency but would not be affected by urea or CHAPS (Annis *et al*, 2005). Therefore, it is the relative changes in accessibility to IASD resulting from added urea

and CHAPS that enable assignment of the environment of individual cysteine residues.

Some of the Bax mutants with a single cysteine in α2, α3, and α4, including F92C and F93C with the aromatic residues in α4 replaced by cysteine, were labeled by IASD in the absence of CHAPS and urea, and the labeling was not increased in the presence of CHAPS, urea, or both (Fig 2B). Thus, these residues are surface exposed. Other Bax mutants, such as L59C, L63C, I66C, and L70C with the cysteine positioned on the hydrophobic side of the amphipathic α2, and F100C with the cysteine replacing the last aromatic residue in α4, were partially labeled by IASD in the absence of CHAPS and urea, and addition of CHAPS, urea, or both resulted in an increase of IASD labeling. To quantify the extent of burial in the MOM, we measured the fraction of IASD labeling for each cysteine in the presence of urea and in the presence of both urea and CHAPS, and then subtracted the former from the latter to get a membrane burial index, as described in Appendix Fig S3A. The resulting membrane burial indices of all the cysteines shown in Appendix Fig S3B were then normalized to that of G179C, a residue in α9 that is mostly embedded in the MOM as shown by the data in Fig 5 and our previous study (Annis *et al*, 2005). The resulting relative membrane burial indices shown in Fig 2C indicate that at least for a fraction of the mitochondrial Bax proteins, their α2, α3, and α4 are located on the MOM surface with some residues exposed to aqueous milieu as their membrane burial indices are < 40% of that for the membrane-buried reference Gly[179], and they are also not buried in the protein (see below). Other residues, particularly the four hydrophobic residues on one side of α2 and the one aromatic residue at the C-terminus of α4, are buried in the MOM as their membrane burial indices are more than 40% of that for Gly[179] (Fig 2A, top-right).

The seven residues in three consecutive helical turns of α5 were buried in the MOM, as evidenced by their IASD-labeling profile (Fig 2B) and relative membrane burial indices (Fig 2C). These results indicate that about three-fifths of the five-turn α5 helix is embedded in the MOM for at least a fraction of the mitochondrial Bax proteins (Fig 2A, bottom-right), consistent with the conclusion about the α5 topology of mitochondrial Bax from apoptotic cells in our previous study (Annis *et al*, 2005) and a recent study by others (Westphal *et al*, 2014a).

The BH3-in-groove crystal structure predicts that many non-polar and a few polar residues, such as the eight residues shown in Fig 2A, bottom-left, would be buried in the dimer interface. To examine this, we subtracted the fraction of IASD labeling of each single-cysteine mutant in the presence CHAPS from that in the presence of both urea and CHAPS to derive a protein burial index indicating the extent of burial of the cysteine in the protein complex. The resulting protein burial indices of all the cysteines shown in Appendix Fig S3C were then normalized to that of Y115C, a residue that is buried in the hydrophobic core of BH3-in-groove dimer crystal structure (PDB entry 4BDU), and that is also the most protein-buried residue in mitochondria-bound Bax according to the protein burial index. The resulting relative protein burial indices shown in Fig 2D suggest that six of the eight predicted protein-buried residues, including Leu[63], Ile[66], and Leu[70] in α2, Met[79] in α3, and Val[111] and Tyr[115] in α5, are indeed buried in the protein complex for at least a fraction of the mitochondrial Bax proteins, as their protein burial indices are more than 40% of that for the protein-buried reference residue Tyr[115] (Fig 2D). Of the other two residues, Leu[59]

is buried in the MOM, whereas Leu[76] is exposed to the aqueous milieu. In addition, Lys[119] and Val[121] in α5 are buried in the protein complex at mitochondria, although they are not buried in the BH3-in-groove dimer crystal structure, likely due to the unfolding of the last two helical turns in the crystal.

Based on all the data presented so far, we conclude that a fraction of mitochondrial Bax proteins formed a dimer interface similar to that shown in the BH3-in-groove dimer crystal structure. However, in another fraction of mitochondrial Bax, α5 is partially embedded in the MOM, separating from α2, α3, and α4 on the MOM surface. This conclusion is also consistent with the observation that some of the protein-buried residues such as Leu[63], Leu[66], and Leu[70] in α2, and Tyr[115] and Lys[119] in α5 are also buried in the membrane. Thus, the protein burial of these residues occurs in one fraction of Bax molecules that is in the BH3-in-groove dimer conformation on the membrane surface, while the membrane burial of the same residues takes place in the rest of the Bax molecules that are more deeply embedded in the membrane.

After the departure of α5, the remnant BH3-in-groove dimer interface is rearranged to another conformation

Insertion of α5 into the MOM would peel it off from the rest of the BH3-in-groove dimer structure remaining on the membrane surface. This conformational change might destabilize the dimer structure and initiate additional conformational changes to rearrange the structure to a more stable conformation. To test this hypothesis, we performed a MD simulation, starting with the BH3-in-groove dimer structure on the surface of a lipid bilayer comprised of MOM characteristic phospholipids (Kuwana *et al*, 2002), and then moving the two α5 helices into the bilayer as described in Appendix Supplementary Methods and Appendix Table S1. The simulation disclosed a dynamic dimer structure in which the α2-α3-α4 regions remain on the bilayer surface (Appendix Fig S4A). Several residues that were initially distal in the interface became proximal during the simulation (Appendix Fig S4B). To determine whether the simulated conformational changes indeed happen in the Bax proteins bound to mitochondria, we made more Bax mutants with single or double cysteines replacing the interfacial residues that either approached one another or remained separated during the simulation. All of these Bax mutants generated disulfide-linked Bax dimers after they were activated and integrated into the Bax⁻/⁻/Bak⁻/⁻ MOM (Fig 3A–C and EV4; Appendix Fig S2B), suggesting that the BH3-in-groove dimer interface remained on the membrane surface was altering such that the respective cysteines were close enough to form a disulfide, as the MD simulation predicted. Note that the C62 and S72C mutants also generated a disulfide-linked dimer even though the two residues never reached a disulfide-linkable distance during the 135-ns simulation. These results suggest that after binding to membranes, the Bax dimer interface seen in the crystal rearranges, and the scale of the conformational changes is larger than that can be sampled within this short simulation time.

To search for a rearranged BH3-in-groove dimer interface that fits all the crosslinking data in Figs 3 and EV4, we performed a global computational search for a model that simultaneously optimized for the distance between the crosslinked positions and the chemical geometry of the interfacial residues. In particular, we allowed the three helices α2, α3, and α4 to move freely in space driven by the
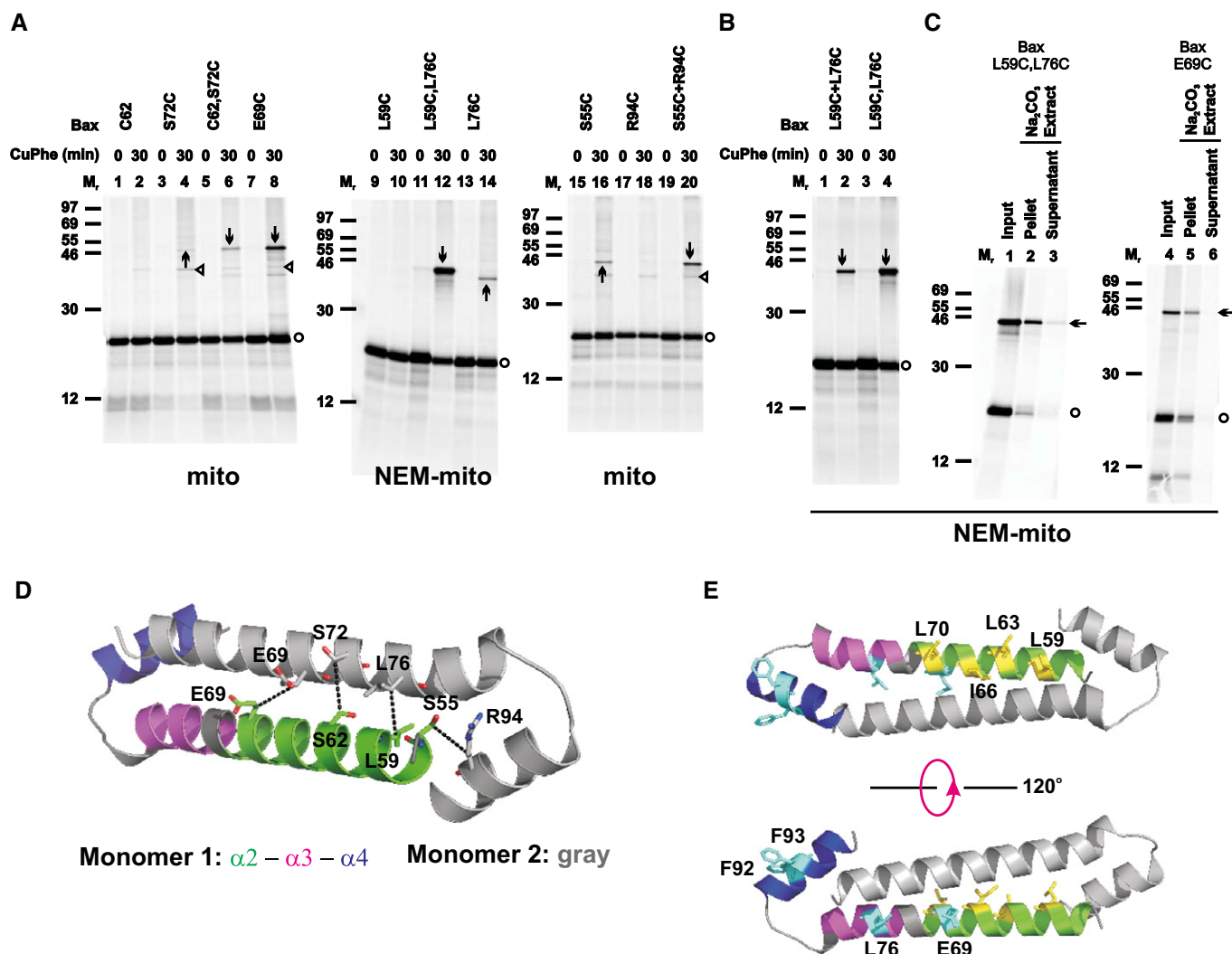
Figure 3.   The BH3-in-groove dimer interface rearranges to form a helices α2-α3-α4 dimer interface.

A, B   Oxidized mitochondria with the radioactive single- or double-cysteine Bax proteins, or the single-cysteine Bax protein pairs were prepared and analyzed as in Fig 1B.

C   Oxidized mitochondria with the radioactive double-cysteine Bax protein were prepared, subjected to Na₂CO₃ extraction, and analyzed as in Fig 1D.

D   The best structural model for the helices α2-α3-α4 dimer is shown with the residue pairs replaced by cysteine pairs in (B) presented in stick form. The β-carbon atoms of each residue pair are linked by a dashed line with the distance ranging from 4.7 to 5.2 Å.

E   The structural model for the α2-α3-α4 dimer is shown with the residues that are buried in the MOM or exposed to the aqueous milieu as determined in Fig 2 presented in yellow or cyan stick form, respectively. The pdb file for the model is provided as Dataset EV1 and named as "Helices a2-a3-a4 dimer.pdb".

Data information: In (D–E), the color codes for the two monomers are indicated. In (A–C), protein standards, Bax monomers, and disulfide-linked Bax dimers are indicated as in Fig 1B. In some targeting reactions, the mitochondria were pretreated with NEM (NEM-mito), while in others the mitochondria were untreated (mito). In (A and B), n = 2 for C62,S72C, R94C, and L59C+L76C; 3 for S72C, S55C, and S55C+R94C; 4 for C62; 6 for E69C, L59C, and L76C; 8 for L59C,L76C. In (C), n = 2 for each mutant. The triangle-indicated bands generated from the untreated mitochondria in (A) are disulfide-linked heterodimers between the Bax cysteine mutants and unknown mitochondrial proteins, as they disappeared if the mitochondria were pretreated with NEM to block the sulfhydryls of the mitochondrial proteins before adding the Bax mutants (e.g., compare the products from E69C at the untreated mitochondria in lane 8 of Fig 3A to those from the same mutant at the NEM-pretreated mitochondria in lane 4 of Fig 3C, or the products from S72C at the untreated mitochondria in lane 4 of Fig 3A to those from the same mutant at the NEM-pretreated mitochondria in lane 4 of Fig EV4A). In contrast, the disulfide-linked Bax homodimers were still formed in the NEM-pretreated mitochondria (e.g., the arrow-marked band in lane 4 of Fig 3C and lane 4 of Fig EV4A).

Source data are available online for this figure.

optimization of distance constraints derived from the crosslinking data. The search produced a model in which helices α2 and α3 are merged into a single helix forming a homodimer in a conformation that resembles an antiparallel coiled coil, whereas α4 folds back after a loop capping the end of the coil (Fig 3D). This α2-α3-α4

dimer model has excellent packing and satisfies all imposed experimental constraints, with the β-carbon distances near 5 Å for all the disulfide-linkable residue pairs. A similarly extended α2-α3 single helix was observed before in the structure of a Bax BH3 peptide (residues 54–73 or 54–79) in complex with either a domain-swapped

Bax dimer (PDB entry 4BD6) (Czabotar *et al*, 2013) or a Bcl-XL monomer (PDB entry 3PL7) (Czabotar *et al*, 2011). Moreover, one side of the dimer can be embedded in the MOM, whereas the other side of the dimer is exposed to the aqueous milieu (Fig 3E), consistent with the conclusion drawn from the IASD-labeling data (Fig 2).

Formation of the α2-α3-α4 interface depends on prior formation of the BH3-in-groove interface

According to the BH3-in-groove dimer structure, Gly[108] in the groove makes van der Waals' contacts with Gly[67] and Asp[71] in the BH3 region, thereby contributing to the overall stability of the dimer (Fig 4A, left). Gly[108] to glutamate mutation (G108E) would not only eliminate these favorable interactions, but also generate steric clashes with the Gly[67], Leu[70], and Asp[71], and electrostatic repulsions with the Asp[68] and Asp[71] (Fig 4A, right). In fact, a previous study showed that the G108E mutation inhibited Bax oligomerization and MOMP activity even in the presence of another mutation, Ser[184] to valine (S184V), that targeted the G108E mutant to mitochondria (Kim *et al*, 2009). To determine whether the G108E mutation disrupts the BH3-in-groove interface formed by the mitochondria-bound Bax, we put it together with the S184V mutation into the single- or double-cysteine Bax mutants that could generate disulfide-linked dimers according to the BH3-in-groove dimer structure. The experiments with these mutants showed that the G108E mutation inhibited the disulfide formation along the entire BH3-in-groove interface (Fig 4B), suggesting that the mutation disrupts the dimer interface.

The previous study also showed that a Bax with G108E and L63E double mutations did not bind to tBid, but Bax with an L63E single mutation did (Kim *et al*, 2009). Because the L63E mutation also targeted Bax to mitochondria even in the presence of the G108E mutation, the authors concluded that the G108E mutation in the groove disrupted tBid binding to mitochondrial Bax, a step that would be upstream of Bax oligomerization. Therefore, it is conceivable that the G108E mutation does not directly disrupt the BH3-in-groove Bax homodimerization but does so indirectly by blocking the tBid–Bax heterodimerization that induces Bax homodimerization. To test this hypothesis, we performed disulfide crosslinking of tBid L105C, a mutant with the single cysteine located near the BH3 region, with Bax E69C, a mutant with the single cysteine in the BH3-binding groove. As expected from the Bid BH3 peptide–BaxΔα9

complex structure (PDB entry 4BD2) (Czabotar *et al*, 2013), and hence a positive control, a disulfide-linked dimer with a M_r expected for the tBid–Bax heterodimer was detected in the mitochondria together with tBid and Bax monomers and a disulfide-linked Bax homodimer (Fig 4C, lane 2). The identity of the tBid–Bax heterodimer was confirmed by reciprocal immunoprecipitation with tBid- or Bax-specific antibodies (lanes 3 and 4). Surprisingly, when the G108E mutation was introduced into the Bax E69C together with the S184V mutation that targets Bax to the mitochondria, the disulfide-linked tBid–Bax heterodimer was still formed (lanes 10–12), just like the other control, Bax E69C with the S184V mutation (lanes 6–8). As expected, the formation of the disulfide-linked Bax homodimer was inhibited by the G108E mutation. These data demonstrate that the G108E mutation in Bax does not disrupt the interaction with tBid, and hence, the inhibitory effect of this mutation on the BH3-in-groove Bax homodimerization is direct. The mutation also does not interfere with the overall folding of Bax, because the mutant Bax retains the capacity to bind tBid. The previous observation that the G108E mutation disrupts Bax-tBid interaction is likely due to an additional impact from the second mutation, L63E.

To determine whether the α2-α3-α4 Bax homodimer can still form even when the BH3-in-groove homodimer is disrupted, we tested the effect of the G108E mutation on the disulfide crosslinking via the α2-α3-α4 interface. The results (Fig 4D) suggest that the G108E mutation entirely abolishes the formation of the α2-α3-α4 interface. Because Gly[108] is the first residue of α5 that is not part of the α2-α3-α4 dimer (Fig 3D), one does not expect the G108E mutation to disrupt this dimer directly. Further, the mutation does not disrupt the tBid–Bax interaction on which the α2-α3-α4 dimerization may depend. Therefore, elimination of α2-α3-α4 dimerization by the G108E mutation suggests that the α2-α3-α4 dimerization depends on the BH3-in-groove dimerization, a prediction from the model in which the BH3-in-groove dimerization is upstream of, and required for, other interactions that further oligomerize Bax at the MOM (Czabotar *et al*, 2013).

Helix α9 inside the MOM forms a dimer interface that has two conformations

Previous studies suggested that α9 is inserted into the MOM after Bax is activated (Annis *et al*, 2005; Westphal *et al*, 2014a). Whether

---

Figure 4. G108E mutation in the groove disrupts the BH3-in-groove as well as the helices α2-α3-α4 Bax homodimer interface, but not tBid–Bax heterodimer interface. ▶

A   Left panel, part of the BH3-in-groove dimer structure is shown with Gly[108] from one monomer presented in sphere form, and Gly[67] and Leu[70] from the other monomer that have van der Waals' contacts with the Gly[108] presented in stick form. Asp[68] and Asp[71] from the other monomer are also presented in stick form. Right panel, the same structure is shown with the Gly[108] changed to glutamate (G108E), which results in steric clashes with the Gly[67], Leu[70], and Asp[71], and electrostatic repulsions with the Asp[68] and Asp[71].

B   The radioactive single- or double-cysteine Bax proteins with or without the indicated mutations were activated and targeted to the mitochondria that were either untreated (mito) or pretreated with NEM (NEM-mito), then oxidized and analyzed as in Fig 1B. Protein standards, and monomers and disulfide-linked dimers of the Bax proteins are indicated as in Fig 1B. *n* = 2 for all mutants.

C   The *in vitro* synthesized [35S]Met-labeled Bax E69C protein with or without the additional mutations (G108E and/or S184V) were activated by the *in vitro* synthesized [35S]Met-labeled tBid L105C protein and targeted to the Bax⁻/⁻/Bak⁻/⁻ mitochondria that were pretreated with NEM. The resulting mitochondria were isolated and oxidized by CuPhe for 0 or 30 min. The resulting "0 min" samples (1 equivalent each) and "30 min" samples (1 equivalent each) were analyzed by non-reducing SDS–PAGE and phosphorimaging. The remaining "30 min" samples (4 equivalent each) were immunoprecipitated (IP) by either Bax- or tBid-specific antibody, and then analyzed by non-reducing SDS–PAGE and phosphorimaging. The identities of the four major products, indicated on the right side of the image, were based on their M_r and recognition by the respective antibody. *n* = 2.

D   The disulfide crosslinking data were obtained from the indicated Bax mutants and presented as in (B). *n* = 2 for all mutants.
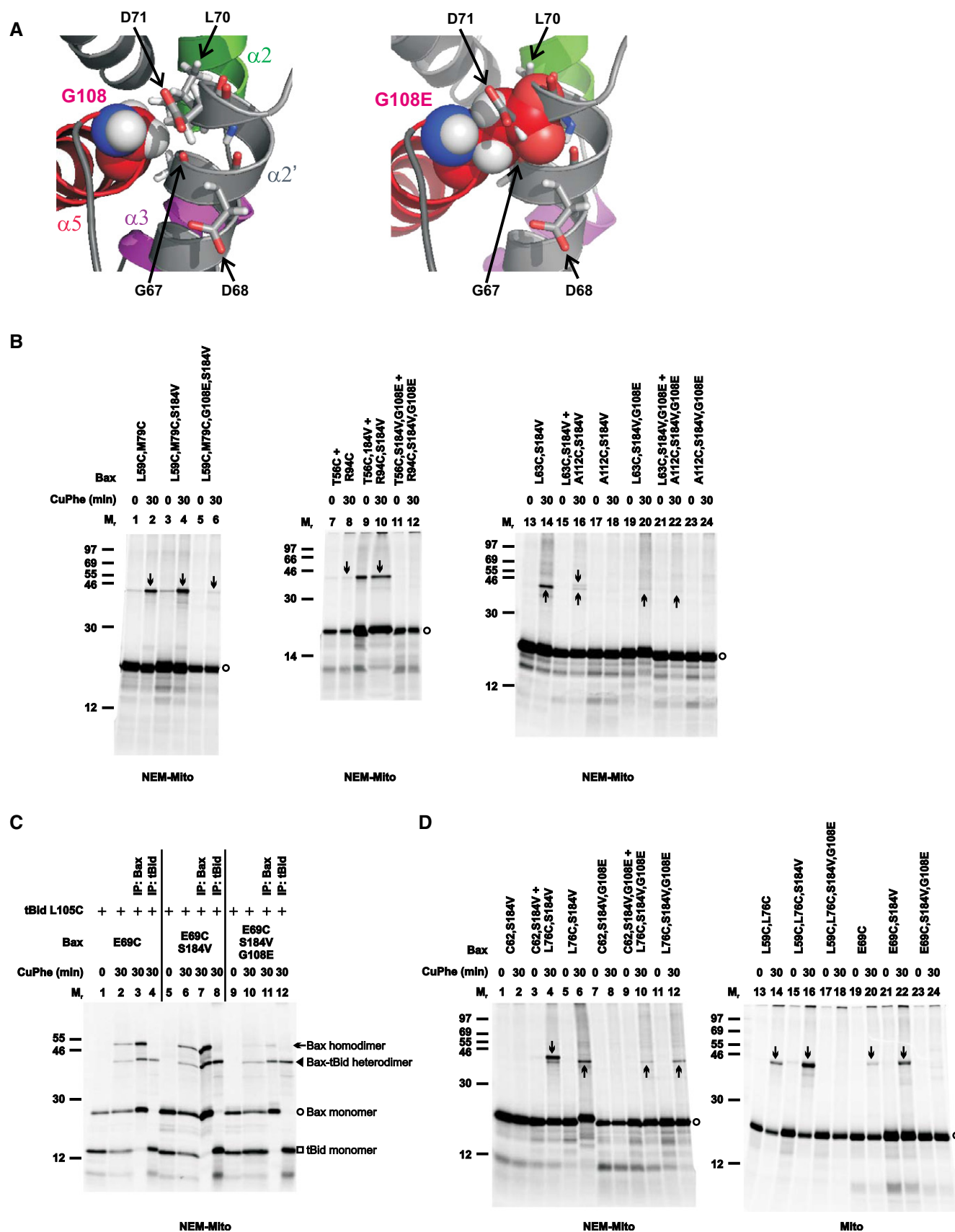
Source data are available online for this figure.

Figure 4.

the insertion results in a partially or fully embedded helix in the MOM is unknown. To determine the membrane topology of α9, we constructed ten Bax mutants with single cysteines positioned throughout α9 and did the IASD-labeling experiment after activating and targeting the Bax mutants to the $Bax^{-/-}/Bak^{-/-}$ mitochondria. The results (Fig 5A; Appendix Fig S5) show that seven residues in the middle three turns of α9 helix are embedded in the MOM, as evidenced by their relative membrane burial indices being 40% or more of that of the membrane-buried reference Gly^{179} (Fig 5B). In contrast, the relative membrane and protein burial indices of two residues in the N-terminal two turns and one residue in the C-terminal turn are < 40% of that of the respective reference Gly^{179} and Tyr^{115} (Fig 5B and C), indicating that these parts of α9 are exposed to aqueous milieu. Therefore, like α5, α9 is partially embedded in the MOM in a fraction of the activated mitochondrial Bax molecules (Fig 5D).

Sequence analysis of α9 revealed a GxxxA motif in the C-terminal half (Gly^{179}-Val-Leu-Thr-Ala^{183}; Fig EV1A). GxxxG and GxxxG-like motifs are often found in transmembrane domains and are known to promote dimerization (Russ & Engelman, 2000; Senes *et al*, 2000).
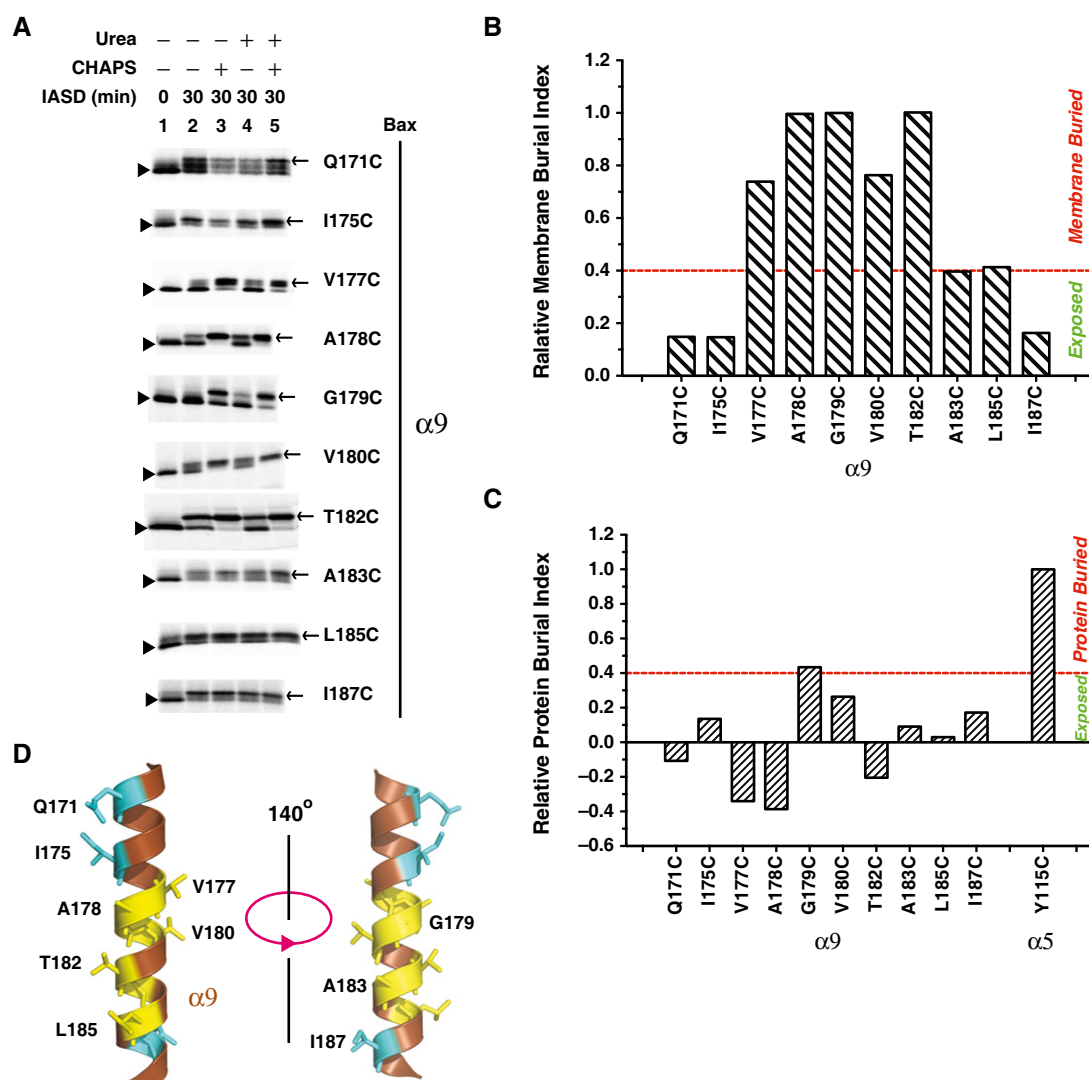

Figure 5. Helix α9 is partially embedded in the MOM.

A   The *in vitro* synthesized radioactive Bax proteins, each with a single cysteine positioned in α9, were activated and targeted to the mitochondria, and labeled with IASD as in Fig 2B. The IASD-labeled and unlabeled Bax proteins were resolved using gradient SDS–PAGE, detected by phosphorimaging and indicated by triangles and arrows, respectively. For all mutants, *n* = 2, except for A183C, *n* = 3.

B, C   The IASD-labeling data in (A) and the similar data from the independent replicates were quantified to derive the membrane or protein burial indices shown in Appendix Fig S5, from which the relative membrane (B) or protein (C) burial indices were obtained as described in Fig 2C and D, and shown.

D   The structure of α9 (extracted from the NMR structure of Bax monomer, PDB entry 1F16) is shown with the residues that are buried in the MOM or exposed to the aqueous milieu, as the IASD-labeling data in (A–C) suggested, presented in yellow or cyan stick form, respectively.

Source data are available online for this figure.

In particular, the GxxxG-like motifs are involved in homodimerization of transmembrane helices from glycophorin A and a BH3-only protein Bnip-3 (MacKenzie *et al*, 1997; Sulistijo & Mackenzie, 2009). To investigate the hypothesis that the GxxxA motif mediates homodimerization of Bax α9 in the MOM as previously observed (Bleicken *et al*, 2014; Gahl *et al*, 2014; Iyer *et al*, 2015), we built a homodimer model for the α9 using the program CATM (Mueller *et al*, 2014). We tested the model by generating single-cysteine Bax mutants with the cysteines positioned in the dimer interface (Fig 6A), and induced the disulfide crosslinking after activating and targeting these mutants to the Bax$^{-/-}$/Bak$^{-/-}$ mitochondria. As predicted by the model, the integral Bax I175C, G179C, A183C, and I187C mutants formed disulfide-linked homodimers (Figs 6B and C, and EV5). Particularly, the cysteine that replaced Ala^{183} of the GxxxA motif yielded the strongest homodimer band among the four cysteines, comparable to the dimers captured by the cysteines in the BH3-in-groove and α2-α3-α4 interfaces (e.g., the disulfide-linked L59C-M79C or C62-L76C dimer in Fig 1B, and E69C-E69C or L59C-L76C dimer in Fig 3A). These data suggest that like the other two dimerizations outside the MOM, GxxxA-mediated α9 dimerization inside the MOM occurs between activated mitochondrial Bax proteins.

To further test the GxxxA α9 dimer model, disulfide crosslinking was performed with other single-cysteine Bax mutants with the cysteines located at nearby positions that would have low propensity to form disulfides according to the model. Four of the Bax mutants (T174C, V177C, V180C, and S184C) did not generate disulfide-linked homodimers, as predicted by the GxxxA model (Fig 6B and D). Unexpectedly, the other four mutants (Q171C, A178C, T182C, and L185C) generated homodimers (Figs 6D and E, and EV5). We therefore identified another dimer model from our computational search that could fit these positive disulfide-crosslinking data. In this alternative dimer model, the two helices are more parallel (thereby termed the parallel α9 dimer model, Fig 6F) in contrast to the GxxxA dimer model, in which the two helices intersect with a right-handed crossing angle of approximately −40° (thereby termed the intersected α9 dimer model, Fig 6A). The parallel α9 dimer model could also accommodate the negative disulfide-crosslinking data from the other four Bax mutants. However, to account for all of the crosslinking data, both models must be correct, suggesting that the disulfide-crosslinking approach identified specific, non-random, yet flexible interactions between the two α9 helices.

A recent FRET study also found a α9 dimer interface after translocation of Bax to the mitochondria in apoptotic cells (Gahl *et al*, 2014). In accordance with the above-mentioned study, our crosslinking data show that both α9 dimers are formed by the Bax proteins that are activated by BH3 protein or peptide and integrated into the MOM (Figs 6C and E, and EV5B–D). To assess the effect of lipids on the dimer structure and stability, we carried out MD simulations, described in Appendix Supplementary Methods and Appendix Table S1, for the α9 dimers in solution containing counterions and in a lipid bilayer comprised of the MOM characteristic lipids, particularly those negatively charged ones known to facilitate Bax activation, insertion, oligomerization, and pore formation (Kuwana *et al*, 2002; Lucken-Ardjomande *et al*, 2008; Shamas-Din *et al*, 2015). We compared the initial conformations of both intersected and parallel α9 dimers (Fig 6A and F), which were generated by the computational modeling and fit the crosslinking data, to the final conformations after 175-ns simulation. The results indicate that both dimer conformations in the lipid bilayer remained stable, with small backbone root-mean-square deviation (RMSD) fluctuations ~1 Å (Appendix Fig S6A, membrane). In contrast, both dimer conformations in the solution became unstable resulting in large backbone RMSD fluctuations ~5 Å and loss of helicity from both termini (Appendix Fig S6A, solution). Therefore, the MD simulation data support an important role for the membrane in stabilizing the α9 dimer structures. Consistent with this prediction, the α9 dimer-specific crosslinking was observed in the mitochondrial fraction after Bax proteins were activated by cBid, but not in the soluble fraction even when cBid was present (Fig EV5D).

To determine the relative stability of the intersected and parallel α9 dimer conformations in the membrane, we did free-energy simulation of α9 dimer transition between the two conformational states. The results suggest that the free energy of the intersected dimer is ~3.5 kcal/mol lower than the parallel one (Appendix Fig S6B). In addition, several intermediate conformational states with different free energy were revealed. In summary, in membranes the intersected α9 dimer is more stable than the parallel dimer, and they may coexist in equilibria with other intermediate dimeric conformations.

The two α9 dimer conformations are formed interdependently, and the formation of both depends on the BH3-in-groove dimerization

The MD simulation data suggest that the two extreme α9 dimer states may be linked through the intermediate states and transitions between them are possible if the energy barriers between them can be surpassed. To determine whether one α9 dimer state could be reached in the absence of the other, we designed one mutation for each interface that would be disruptive to that interface but not the other based on the respective "static" models (Fig 6A and F). The

---

Figure 6. Helix α9 homodimerizes with two interfacial conformations.

A   Structural model for intersected α9 homodimer is shown with one monomer colored brown (α9) and the other gray (α9′). The residue pairs that formed disulfide bonds after they were replaced with cysteine pairs in (B) are presented in stick form, and their β-carbon atoms linked by dashed lines with the distances indicated in Å, except that the Gly^{179} pair is linked by a dashed line via their α carbon atoms with the distance indicated. The pdb files for the model is provided as Dataset EV2 and named as "Helix a9 intersected dimer.pdb".

B–E   The oxidized mitochondria with radioactive single-cysteine Bax proteins were prepared, analyzed as in Fig 1B, and shown in (B) and (D); or subjected to Na$_2$CO$_3$ extraction, analyzed as in Fig 1D, and shown in (C) and (E).

F   Structural model for parallel a9 homodimer is shown with the color codes described in (A). The residue pairs that formed disulfide bonds after they were replaced with cysteine pairs in (D) are presented in stick form, and their b carbon atoms linked by dashed lines with the distances indicated in Å. The pdb files for the model is provided as Dataset EV3 and named as "Helix a9 parallel dimer.pdb".

Data information: In (B–E), protein standards, Bax monomers and disulfide-linked Bax dimers are indicated as in Fig 1B. *n* = 3 for A183C, and A178C; 2 for other mutants.
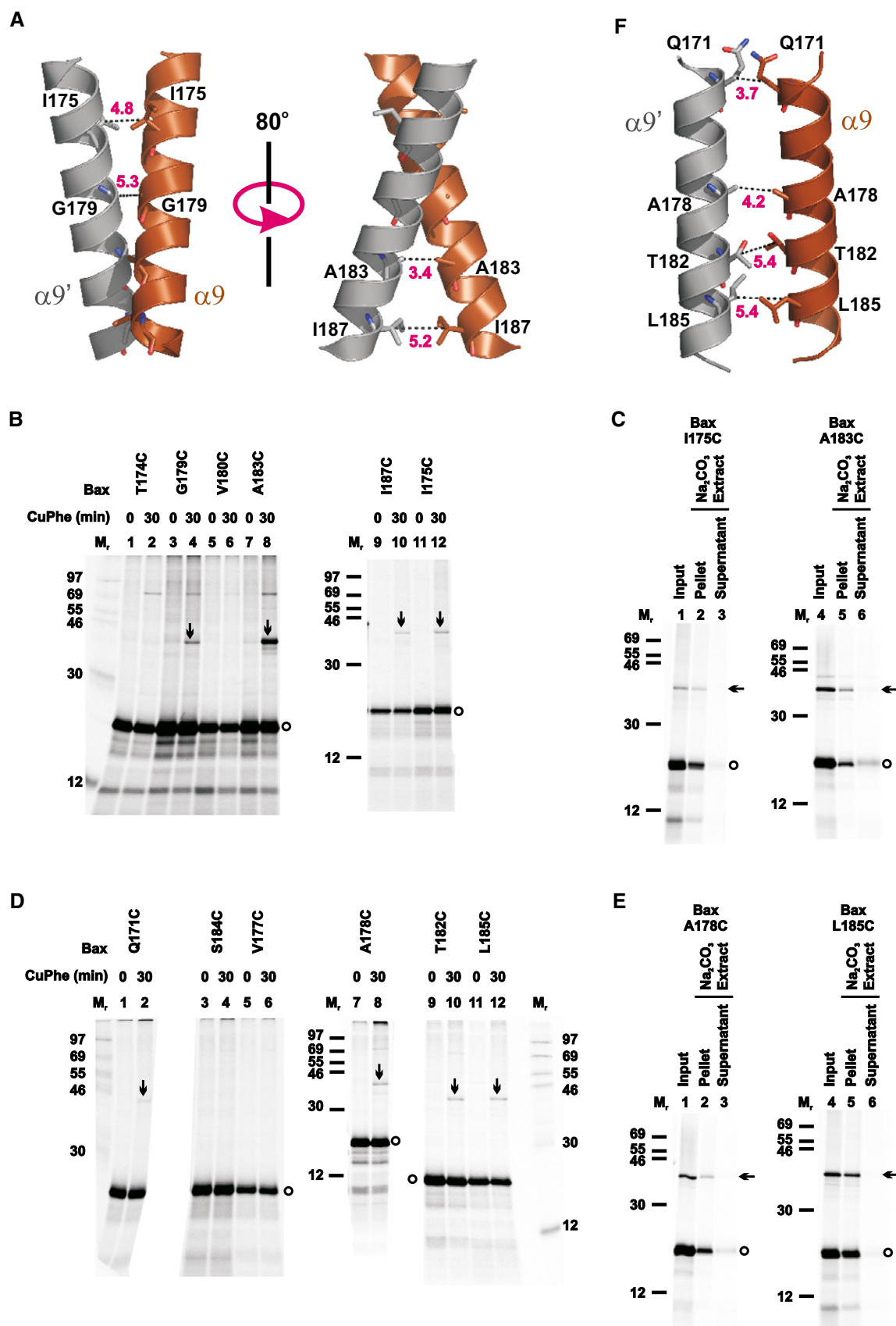
Source data are available online for this figure.

Figure 6.

intersected dimer model predicts van der Waals' interactions between Gly[179] of one α9 and Phe[176] and Val[180] of the other α9 (Fig 7A, intersected α9 dimer, left). Thus, a Gly[179] to isoleucine mutation (G179I) would not only eliminate these favorable interactions but also introduce steric clashes between Ile[179] of one α9 and Phe[176], Ile[179] and Val[180] of the other α9, thereby disrupting the intersected dimer (Fig 7A, intersected α9 dimer, right). The parallel dimer model predicts favorable van der Waals' interactions between Gln[171], Ile[175], Ala[178], Thr[182], and Leu[186] in the two α9 helices. Mutating Thr[182] to isoleucine (T182I) would remove the favorable interaction between the two Thr[182] (Fig 7A, parallel α9 dimer, left) and introduce a steric clash between the two Ile[182] (Fig 7A, parallel α9 dimer, right), thereby disrupting the parallel dimer. Confirming these predictions, the G179I or T182I mutation greatly inhibited the disulfide crosslinking of Bax A183C or A178C that was specific to the intersected or parallel dimer, respectively (Fig 7B, arrow-indicated bands in lane 4 versus lane 2, or lane 8 versus lane 6).

The G179I or T182I mutation also greatly inhibited the disulfide crosslinking of Bax A178C or A183C, respectively (Fig 7B, arrow-indicated bands in lane 12 versus lane 10, or lane 14 versus lane 16), suggesting that the disruptive mutation in the intersected dimer is also disruptive to the parallel dimer and vice versa. This result was not predicted by the static dimer models, suggesting that the two α9 dimer conformations are formed in an all-or-none fashion or interdependently.

We carried out MD simulations with the α9 dimers containing the G179I or T182I mutation in the membrane to assess the effects of these mutations in a dynamic setting. Comparison of the initial and final structures of the dimers suggests that the G179I mutation disrupts both intersected and parallel dimers, whereas the T182I mutation only disrupts the parallel dimer (Appendix Fig S6C). To compare with the effect of each mutation observed in the crosslinking experiment with the A183C or A178C single-cysteine mutant that captured the intersected or parallel dimer, respectively (Fig 7B), we measured the β-carbon distance between the two Ala[183] residues or between the two Ala[178] residues in the two α9 dimers with the G179I or T182I mutation in the initial and final structures. The results indicate that the G179I mutation increases the β-carbon distance for both residue pairs (Appendix Fig S6C), thereby explaining its inhibitory effect on the disulfide crosslinking of both A183C and A178C mutants. In contrast, the T182I mutation only increases the β-carbon distance for the Ala[178] residue pair significantly, thereby only explaining its inhibition of the A178C crosslinking. While the inhibition of the A183C crosslinking or the intersected α9 dimerization by the T182I mutation can be explained by neither the MD simulation nor the static modeling, it remains possible that the intersected α9 dimer with the lowest free energy may be evolved from the parallel dimer through the intermediate conformational states revealed by the free-energy simulation of the transition (Appendix Fig S6B). And if so, blocking the upstream parallel dimerization by the T182I mutation may also block the downstream intersected dimerization.

The model that the BH3-in-groove dimerization is a nucleation event that initiates other dimerizations to further oligomerize Bax predicts that the α9 dimerization would depend on the BH3-in-groove dimerization (Czabotar *et al*, 2013). To verify this prediction, we tested the effect of the G108E mutation that disrupted the BH3-in-groove dimerization on the α9 dimerization. The G108E mutation completely abolished the homo-disulfide crosslinking of

both Bax A183C and A178C that specifically captured the two conformations of the α9 dimer, respectively, even though both Bax mutants were targeted to the mitochondria by the S184V mutation in α9, which by itself did not abolish the homo-disulfide crosslinking (Fig 7C, disappearance of the arrow-indicated bands from lanes 6 and 12, but not lanes 4 and 10). These data suggest that α9 dimerization does not occur in the absence of the BH3-in-groove dimerization, thereby placing the α9 dimerization downstream of, and dependent on, the BH3-in-groove dimerization.

In contrast, the G179I mutation that disrupted the α9 dimerization via both conformations did not affect the BH3-in-groove dimerization as captured by the disulfide linkage of Bax L59C,M79C (Fig 7D, arrow-indicated bands in lane 2 versus lane 4). The G179I mutation also did not reduce the α2-α3-α4 dimerization as detected by the disulfide linkage of Bax L59C,L76C (Fig 7D, arrow-indicated bands in lane 8 versus lane 6). Thus, both BH3-in-groove and α2-α3-α4 dimer interfaces are formed in the absence of α9 dimerization, as expected from the model that places the BH3-in-groove and the α2-α3-α4 dimerizations upstream of the α9 dimerization.

The α9 dimerization links the BH3-in-groove or the α2-α3-α4 dimer into higher order oligomers

The oligomerization of Bax requires at least two separate dimer interfaces. To determine whether the BH3-in-groove or the α2-α3-α4 dimer interface located on the MOM and the intersected or parallel α9 dimer interface located in the MOM could mediate oligomerization of Bax dimers, we generated Bax mutants with three cysteines. The first two cysteines, L59C and M79C or L59C and L76C, were positioned in the BH3-in-groove or the α2-α3-α4 dimer interface, and the third cysteine, A183C or A178C, was positioned in the intersected or the parallel α9 dimer interface, respectively. After activating and targeting to the Bax^{−/−}/Bak^{−/−} mitochondria, and oxidizing by CuPhe, each of these triple-cysteine Bax mutants formed multiple products with M_r higher than the monomers (Fig 8A, lanes 4, 10, 16, and 22, indicated by arrows, and open and closed triangles). The products with the M_r below 46 are the disulfide-linked Bax homodimers, because they were also formed by the corresponding double- or single-cysteine Bax mutant (lanes 2, 6, 8, 12, 14, 18, 20, and 24, indicated by arrows). The product with the M_r above 69 formed by the triple-cysteine Bax mutants containing A178C or A183C is not a disulfide-linked dimer, because it could not be reduced (compare open triangle-indicated band in lanes 4 and 10 of non-reducing gel to that in the respective lanes of reducing gel). The remaining products (lanes 4, 10, 16, and 22) indicated by closed triangles) are the disulfide-linked Bax oligomers, as judged by their M_r and disappearance on the reducing gel. These products were detected only in the samples containing the triple-cysteine mutants but not those containing the double- or single-cysteine mutants, suggesting that the two disulfides in the BH3-in-groove or the α2-α3-α4 dimer interface together with the one disulfide in the intersected or the parallel α9 dimer interface linked Bax monomers into oligomers. Together, these results suggest that the α2, α3, and α4 with or without α5 formed a dimer interface that was separated from another dimer interface formed by the α9, and that the two dimer interfaces together mediated Bax oligomerization.
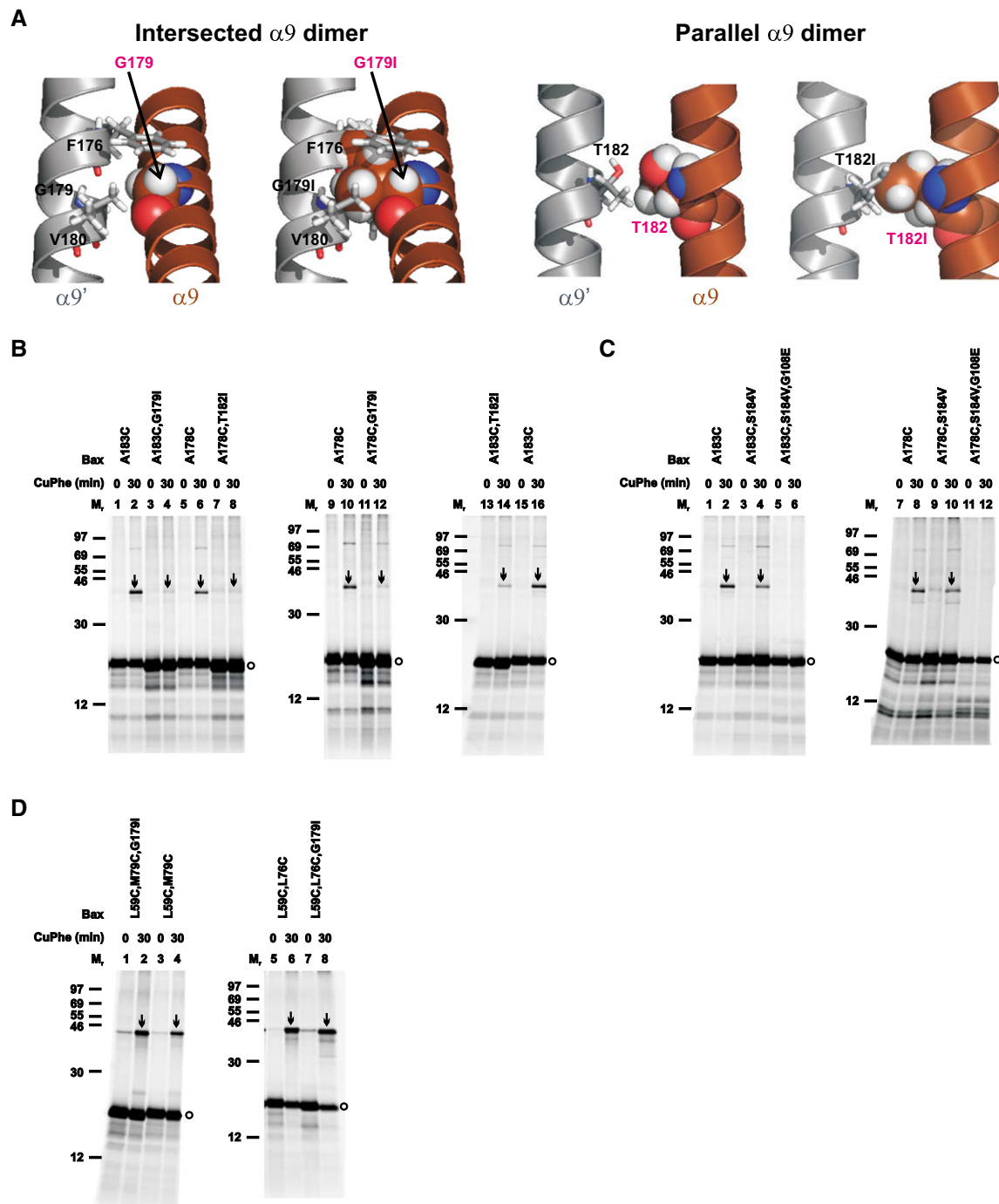
Figure 7. G179I or T182I mutation in α9 disrupts the α9 dimer but not the BH3-in-groove and α2-α3-α4 dimers, whereas G108E mutation in the groove disrupts the α9 dimer.

A   Intersected α9 dimer: the structural model on the left depicts one monomer with Gly^{179} in sphere form, and the other monomer with Phe^{176}, Gly^{179}, and Val^{180} that have van der Waals' contacts with the first Gly^{179} in stick form. The same model is shown on the right, except that the two Gly^{179} are changed to isoleucine (G179I), which results in steric clashes between the Ile^{179} in one monomer and the Phe^{176}, Ile^{179} and Val^{180} in the other monomer, and vice versa. Parallel α9 dimer: the structural model on the left depicts the two interfacial Thr^{182} that have van der Waals' contacts in sphere or stick form. The same model is shown on the right, except that the two Thr^{182} are changed to isoleucine (T182I), which results in a steric clash with each other.

B–D   The *in vitro* synthesized radioactive single- or double-cysteine Bax proteins with or without the indicated mutations were activated and targeted to the mitochondria, oxidized, and analyzed as in Fig 1B. Protein standards, and monomers and disulfide-linked dimers of the Bax proteins are indicated as in Fig 1B. *n* = 2 for all mutants.

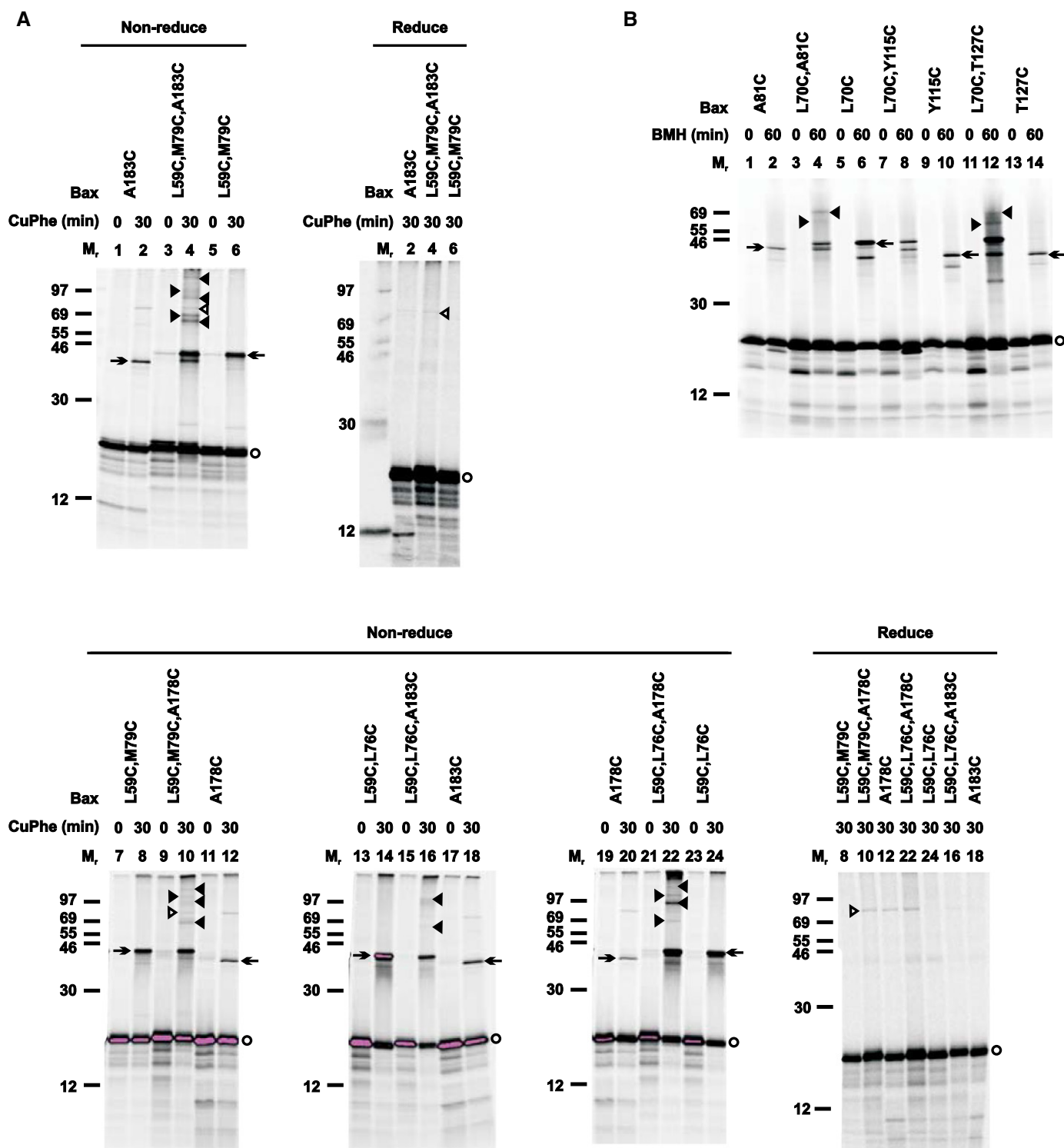Source data are available online for this figure.

Figure 8. Combinations of either the BH3-in-groove or the α2–α3–α4 dimer interface with the α9 dimer interface mediate Bax oligomerization.

A   The oxidized mitochondria with radioactive single-, double-, or triple-cysteine Bax proteins were prepared and analyzed by non-reducing or reducing SDS–PAGE as in Fig 1B. Protein standards, Bax monomers, and disulfide-linked Bax homodimers are also indicated as in Fig 1B. Closed triangles indicate disulfide-linked higher order Bax homo-oligomers. Open triangles indicate a background band that could not be reduced, and hence is not a disulfide-linked complex.

B   The BMH-treated mitochondria with the radioactive single- and double-cysteine Bax proteins were prepared and analyzed as in Fig EV3G, except that closed triangles indicate the BMH-linked Bax oligomers.

Data information: In (A, B), *n* = 2 for all mutants.

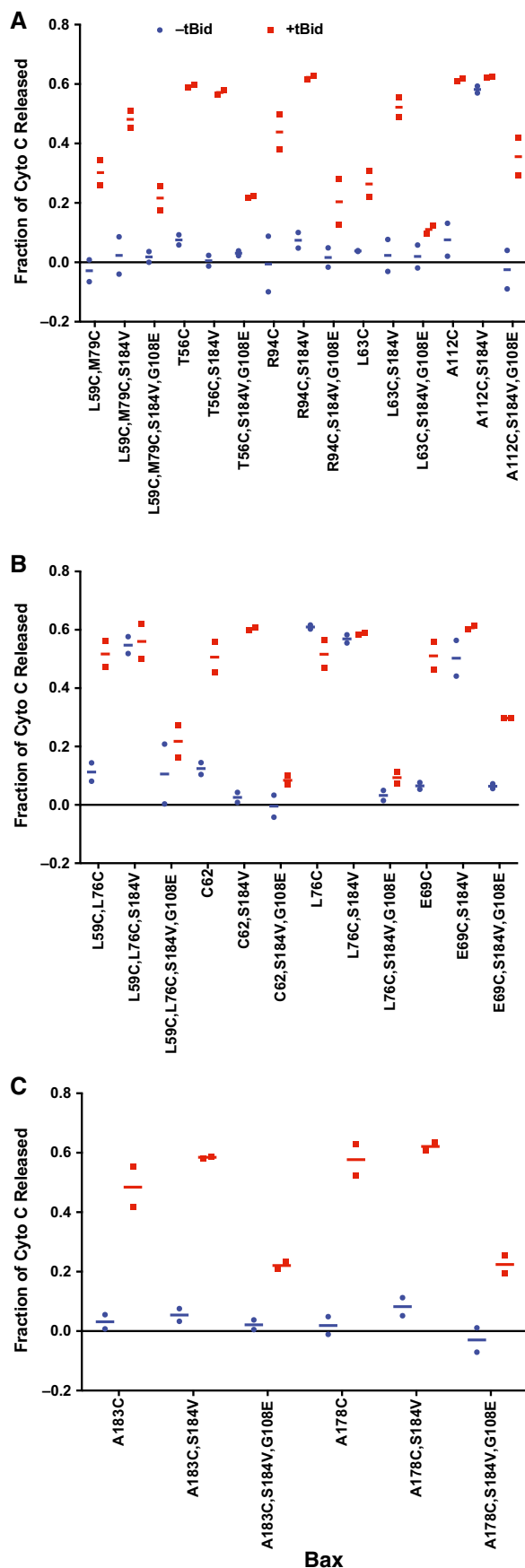Source data are available online for this figure.

Figure 9. The BH3-in-groove dimerization is required for Bax to permeabilize the MOM.

A–C   The single- or double-cysteine Bax proteins with or without the indicated mutations were synthesized *in vitro*, activated by tBid protein and targeted to the Bax⁻/⁻/Bak⁻/⁻ mitochondria. Cytochrome c release from the mitochondria was measured using ELISA. The dots are the fractions of cytochrome c release from two independent replicates after they were corrected as described in Fig EV1B, and the lines are the averages. The amount of the Bax mutants bound to the mitochondria in the assay was determined and the results are shown in Appendix Fig S1.

A DEER study of a liposome-bound Bak complex suggested proximity between two BH3-in-groove dimers, particularly the C-termini of the α3 and α5 helices (Aluvila *et al*, 2014). To determine whether the mitochondrion-bound Bax complex adapts a similar configuration, we used BMH to crosslink the active mitochondrial Bax mutant A81C or T127C with the single cysteine located at the C-terminus of either α3 or α5, respectively. The results show that BMH could link each Bax mutant to a homodimer (Fig 8B, lanes 2 and 14, indicated by arrow). Because the distance between the two Ala[81] or the two Thr[127] is longer than 35 Å according to the BH3-in-groove dimer structure (Czabotar *et al*, 2013) and the DEER-derived Bax dimer model (Bleicken *et al*, 2014), the BMH linkage would not form intradimerically. Instead, the BMH linkage should form interdimerically, if the neighboring BH3-in-groove dimers are in proximity. If this is true, one of these interdimer BMH linkages plus an intradimer BMH linkage (e.g., via the L70C shown in Fig EV3G and H) should produce higher order oligomers. This prediction was confirmed by the BMH crosslinking of two double-cysteine mutants with one cysteine (L70C) forming the intradimer linkage and the other (A81C or T127C) forming the interdimer linkage, and both linkages together forming high order oligomers (Fig 8B, lanes 4 and 12, indicated by closed triangles). As a control, another double-cysteine mutant L70C,Y115C did not form higher order BMH-linked oligomers (Fig 8B, lane 8), because the two BMH linkages are in the same BH3-in-groove dimer (Fig EV3G and H). Taken together, the disulfide and the BMH crosslinking data support a Bax oligomer model in which the BH3-in-groove or α2-α3-α4 dimers are close to each other and linked to higher order oligomers by intersected or parallel α9 dimerization.

The BH3-in-groove dimerization is required for Bax to permeabilize the MOM

To determine which Bax dimer interface is required for assembly of a functional pore in the MOM, we monitored the effect of the interface-disrupting mutations on the MOMP activity of Bax. As shown in Fig 9, the G108E mutation in the BH3-in-groove dimer interface inhibited the tBid-induced and Bax-mediated cytochrome c release from the Bax⁻/⁻/Bak⁻/⁻ mitochondria. This inhibition was not due to the deficiency of Bax binding to mitochondria caused by the G108E mutation, because it occurred in the presence of the S184V mutation that rescued the mitochondrial binding (Appendix Fig S1). This inhibition was caused by the deficiency of Bax dimerization via all of the four interfaces, because the G108E mutation inhibited the formation of all of them as determined by the interface-specific disulfide crosslinking (Figs 4 and 7C). This inhibition is indepen-

Figure 10. **The α9 dimerization is not required for the release of cytochrome c from mitochondria, but facilitates the release of Smac and larger proteins.**

A The cytochrome c release by the indicated Bax mutants was measured, corrected and shown as in Fig 9. The dots are the fractions of cytochrome c release from two independent replicates, and the lines are the means. The amount of the Bax mutants bound to the mitochondria in the assay was determined and the results are shown in Appendix Fig S1.

B Purified wild-type (WT) or mutant (G179I or T182I) Bax protein of the indicated concentration was incubated with the Bax$^{-/-}$/Bak$^{-/-}$ mitochondria in the absence or presence of tBid protein. The proteins released from and those remaining in the mitochondria were separated and analyzed by SDS–PAGE and immunoblotting with antibody specific to either cytochrome c or Smac. *n* = 2.

C Purified wild-type or mutant Bax protein of the indicated concentration alone or together with purified cBid was incubated with the Bax$^{-/-}$/Bak$^{-/-}$ mitochondria containing Smac-mCherry protein. Release of Smac-mCherry was detected by measuring the fluorescence in the supernatant after the mitochondria were pelleted by centrifugation. The dots are the fractions of Smac-mCherry release from three independent replicates, and the lines are the means.

D The *in vitro* synthesized radioactive Bax proteins with indicated mutations were targeted to the mitochondria in the absence or presence of purified tBid protein, and then labeled with IASD, as in Fig 2B. The IASD-labeled and unlabeled Bax proteins were resolved using either gradient SDS–PAGE or IEF, detected by phosphor-imaging, and indicated by arrows and triangles, respectively. *n* = 3 for A178C,G179I; 2 for other mutants.

E The IASD-labeling data in (D) and the similar data from the independent replicates were quantified to derive the membrane burial indices shown in Appendix Fig S7A, from which the relative membrane burial indices were obtained as described in Fig 2C, and shown.

Source data are available online for this figure.

dent of the locations of the cysteines in the Bax mutants (Fig 9) that were used in the disulfide-crosslinking experiments. Some of the Bax mutants (e.g., A112C,S184V and L59C,L76C,S184V) were autoactive, as they released cytochrome c in the absence of tBid. The G108E mutation inhibited the release of cytochrome c by these autoactive Bax mutants and the other Bax mutants that require tBid to activate, suggesting that the inhibition occurred at a step downstream of Bax activation. Consistent with this hypothesis, the G108E mutation did not inhibit Bax interaction with tBid (Fig 4C). Therefore, Bax dimerization via the BH3-in-groove interface that is directly disrupted by the G108E mutation is not only required for dimerizations of Bax via other interfaces including the α2-α3-α4 and the α9 interfaces, but also for the MOMP by Bax.

The α9 dimerization is not required for the formation of small pores in MOM, but facilitates the formation of large pores

To determine the effect of deficient α9 dimerization on Bax MOMP activity, we used the G179I and T182I mutations that abolished the α9 dimerization, but not the BH3-in-groove and α2-α3-α4 dimerizations as shown by the interface-specific disulfide crosslinking (Fig 7B and D; data not shown). These mutations did not reduce the tBid-induced cytochrome c release by Bax with cysteine(s) in any of the four interfaces (Fig 10A). In fact, the G179I mutation made some of these Bax cysteine mutants autoactive, thereby releasing cytochrome c in the absence of tBid.

To verify these results, we purified wild-type Bax protein and mutant Bax protein with either G179I or T182I as the only mutation. We incubated each protein with the Bax$^{-/-}$/Bak$^{-/-}$ mitochondria in the absence or presence of purified tBid protein and monitored the cytochrome c release using immunoblotting. Consistent with the results obtained from the *in vitro* synthesized Bax proteins using the ELISA-based cytochrome c release assay (Fig 10A), the immuno-blots clearly show a tBid-induced cytochrome c release by the purified wild-type Bax protein (Fig 10B, cytochrome c blots, lanes 5 and 6 versus 11 and 12). The result from the T182I mutant at 60 nM was similar to the wild-type protein, but at 120 nM it released cytochrome c in the absence of tBid, and hence was autoactive (lanes 1 and 2 versus 7 and 8). In contrast, the G179I mutant at both concentrations was autoactive, releasing cytochrome c in the absence of tBid (lanes 3 and 4 versus 9 and 10). Therefore, the dimerization of α9 is not required for Bax to form small pores in

the MOM that release cytochrome c, a 12-kDa globular protein with diameter ~30 Å (PDB entry 2AIU) (Liu *et al*, 2006).

We next assayed the release of Smac, a 27-kDa cylinder-like intermembrane space protein with diameter ~25 Å and height ~100 Å (PDB entry 1FEW) (Chai *et al*, 2000) that is released from mitochondria during apoptosis (Du *et al*, 2000; Verhagen *et al*, 2000). As expected, the wild-type Bax released Smac dependent on tBid (Fig 10B, Smac blots, lanes 5 and 6 versus 11 and 12), whereas the G179I mutant released Smac independent of tBid (lanes 3 and 4 versus 9 and 10). Surprisingly, the T182I mutant only released traces of Smac, even at the high concentration and in the presence of tBid (lanes 1 and 2 versus 7 and 8). Therefore, at least one of the α9 dimer-disruptive mutations inhibited the formation of Smac-releasing pores that might be larger than the cytochrome c-releasing pores.

To further test this hypothesis, we monitored the release of Smac-mCherry, a 37-kDa fluorescent fusion protein that contains a cylinder-like GFP fold with diameter ~35 Å and height ~45 Å (PDB entry 1EMA) (Ormo *et al*, 1996) and is localized to the intermembrane space of the mitochondria isolated from the *bax/bak* DKO BMK cells (Shamas-Din *et al*, 2014). By comparing the fluorescence intensities in the supernatant and the mitochondrial pellet, we found that the wild-type Bax released Smac-mCherry in a dose- and cBid-dependent manner (Fig 10C). The G179I mutant also released Smac-mCherry, but independent of cBid, particularly at higher concentrations. In contrast, the T182I mutant released significantly less Smac-mCherry, even at the highest concentration and in the presence of cBid. These data and those from the Smac release assay (Fig 10B) are consistent with the conclusion that α9 dimerization facilitates the formation of large pores in the MOM that release large proteins.

To determine why the G179I and T182I mutations that inhibited the α9 dimerization to the same extent displayed different phenotypes in the large mitochondrial protein release assays, we performed IASD-labeling experiment to examine whether the mutations affect the insertion of α9 and α5 into the MOM. The labeling profiles (Fig 10D) and the membrane burial indices (Fig 10E; Appendix Fig S7A) of wild-type Bax and the two mutants that contain a single-cysteine (A178C) in α9 indicate that the G179I mutation greatly enhanced the α9 insertion into the MOM compared to the wild-type protein, whereas the T182I mutation did not. In contrast, the T182I mutation enhanced the α5 insertion, whereas the
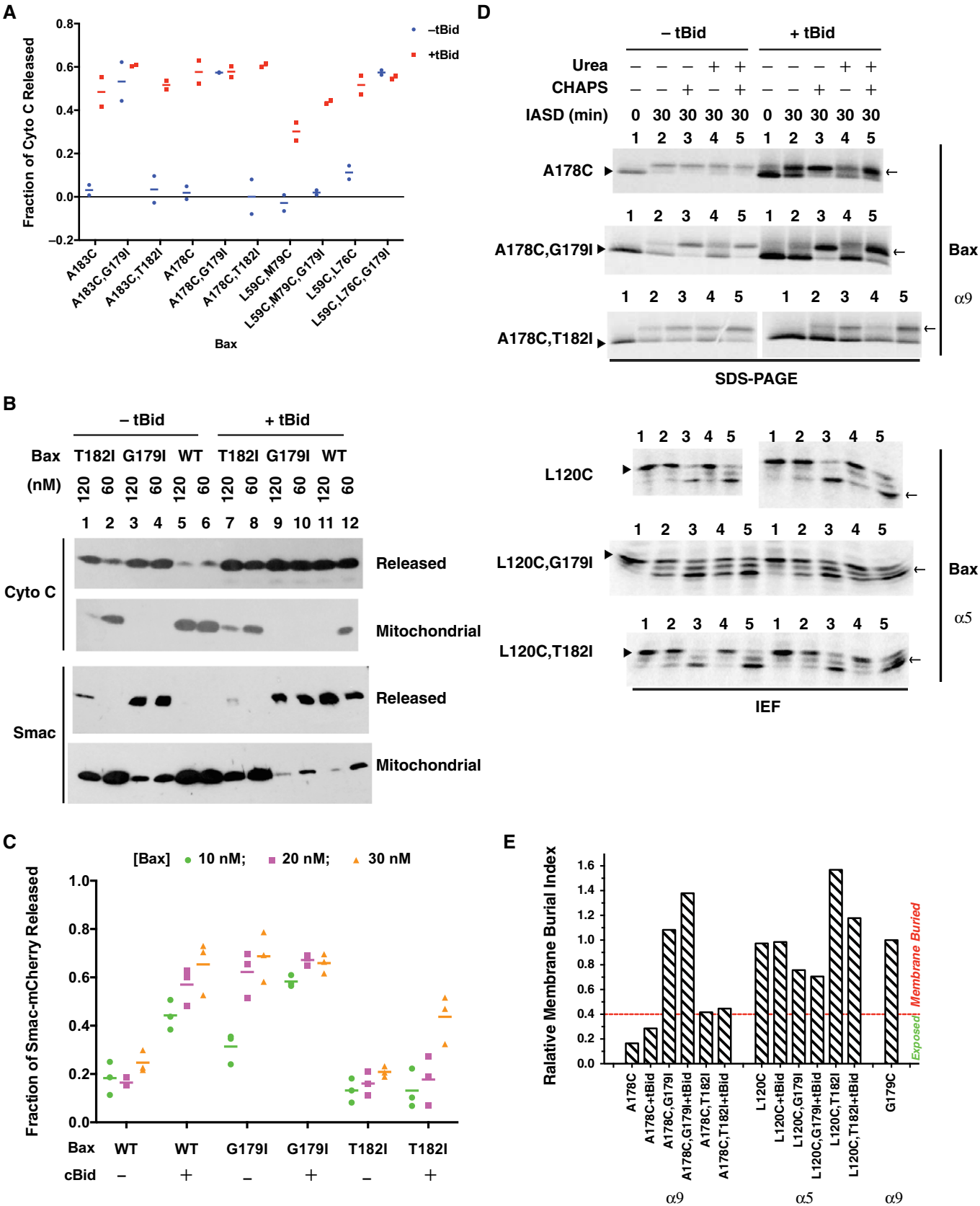
Figure 10.

G179I mutation did not, as shown by the data from Bax L120C with the single cysteine in α5 (Fig 10D and E; Appendix Fig S7A).

We used disulfide crosslinking to assess the effect of G179I mutation on the BH3-in-groove and α2-α3-α4 dimerizations at the mitochondria before and after Bax activation by cBid. The L59C, M79C and the L59C,L76C with the G179I mutation formed the BH3-in-groove and the α2-α3-α4-specific disulfide-linked dimer, respectively, in the mitochondrial pellet fraction in the absence of cBid (Fig EV5E). Dimer formation without cBid is consistent with our data showing that this mutation autoactivates Bax such that it permeabilized the MOM in the absence of tBid. In comparison, dimer formation by the respective cysteine mutants without the G179I mutation in the mitochondrial fraction was cBid dependent (Figs EV3E and EV4D). Intriguingly, a significant dimerization of the L59C,L76C occurred in the post-mitochondrial supernatant fraction (Fig EV4D), which was dramatically enhanced by the G179I mutation but not by cBid or mitochondria or both (Fig EV5E). Whether this dimerization in the soluble fraction contributes to the MOMP activity is uncertain. Nonetheless, increased α9, but not α5, insertion into the MOM can compensate for a deficiency of α9 dimerization, promoting the dimerization on the membrane surface and large pore formation in the membrane. When α9 insertion is at the wild-type level, α9 dimerization facilitates the formation of large pores.

Small pore formation in the MOM is necessary and sufficient for Bax to kill cells

To determine whether the *in vitro* activities of these Bax mutants are relevant to the biological activity of Bax in cells, we expressed wild-type Bax, and the G108E, S184V, G108E/S184V, G179I, and T182I mutants as N-terminal Venus fusion proteins in *bax/bak* DKO BMK cells, and assessed their intracellular localization and apoptotic activity in the absence and presence of STS. Expression levels of these mutants were similar to that of Venus-WT Bax, except for Venus-Bax G108E that had an increased expression (Fig EV2A), which was likely tolerated by the cells since this mutant induced a significantly lower level of apoptosis in the absence and presence of STS when compared to Venus-WT Bax (Fig EV2B). In untreated cells, this mutant was mainly localized to the cytoplasm similar to the wild-type protein (Fig EV2C and D).

Addition of the S184V mutation to Venus-Bax G108E increased the mitochondrial localization resulting in apoptotic activity comparable to wild-type Bax and inducible by STS (Fig EV2B–D). However, the apoptotic activity of the G108E/S184V double mutant was significantly lower than the S184V single mutant (Fig EV2B), even though they had similar mitochondrial localization (Fig EV2C and D). Therefore, the G108E mutation inhibited an activation step downstream of mitochondrial localization of Bax, such as the dimerizations detected by the crosslinking assay above. Furthermore, the residual apoptotic activity of the G108E mutant that could be amplified by the S184V mutation is consistent with the residual dimerizations and cytochrome c release observed *in vitro* (Figs 4 and 9). Together, the results from these mutants in our cell-free and cell-based systems suggest that the G108E mutation incompletely blocks Bax dimerization, MOMP and apoptotic activities especially in the presence of the S184V mutation that targets Bax to the mitochondria.

In contrast, the G179I mutant was constitutively active and spontaneously killed cells (Fig EV2B), an observation that is consistent with those from the *in vitro* MOMP assays (Fig 10A–C). Due to the extensive cell death caused by the G179I mutant, accurate localization data was not obtainable. However, because the cells were dying, Venus-Bax G179I was likely targeted to the mitochondria constitutively, a notion supported by the mitochondrial association of the G179I-containing Bax cysteine mutants observed *in vitro* (Fig EV5E).

When expressed in cells, the T182I mutant had similar localization and slightly higher apoptotic activity compared to that of WT Bax (Fig EV2B–D). While the apoptosis data from the cells expressing the T182I mutant are mostly in line with the cytochrome c release data from the isolated mitochondria reconstituted with the *in vitro* synthesized or purified T182I mutant (Fig 10A and B), the defect of the T182I mutant detected in the *in vitro* Smac and Smac-mCherry release assays (Fig 10B and C) does not translate into a defect in the cell-based apoptosis assay. The most simple explanation is that the cytochrome c release caused by the T182I mutant in the cells is sufficient to induce apoptosis, and the reduction of the Smac release caused by the mutation in the cells is not sufficient to block apoptosis. Therefore, the small pore-forming activity of Bax, which was largely inhibited by the G108E, and enhanced by the G179I, but not altered by the T182I mutation, mirrors the cellular apoptotic activity. The large pore-forming activity, which was inhibited by the T182I mutation, is not required at least for Bax to kill the *bax/bak* DKO BMK cells.

Discussion

In this study, we made several major observations about the conformational changes of activated Bax at the MOM, which are accompanied by a series of protein–protein and protein–membrane interactions, resulting in oligomeric pores that permeabilize the MOM. These observations, together with those published previously, allowed us to propose a mechanistic model by which the activated Bax induces MOMP, as illustrated in Fig 11.

After soluble Bax is activated by a BH3 activator such as tBid and targeted to the MOM (Fig 11A, step I), it inserts into the MOM with either α9 helix alone (step II) or together with α5 and α6 helices (step IV) embedded in the MOM at least partially (Figs 2 and 5) (Annis *et al*, 2005; Lovell *et al*, 2008; Gavathiotis *et al*, 2010; Westphal *et al*, 2014a). Insertion of α9 is favored when the mitochondrial Bax binds to the activator via the canonical BH3-binding groove (step II; Fig 4C) (Kim *et al*, 2009; Czabotar *et al*, 2013), because the release of α9 from the groove empties the groove for the BH3 binding, and the BH3 binding to the groove prevents α9 from reoccupying the groove, thereby keeping α9 in the MOM. In line with this scenario, disruption of α9-groove interaction by the S184V mutation (Suzuki *et al*, 2000) or increase of α9 hydrophobicity by the G179I mutation enhances Bax mitochondrial targeting, MOMP and apoptotic activities (Figs 9, 10, EV2 and EV5E). When the BH3 activator dissociates from the groove, insertion of α5 and α6 is favored (step IV), because the empty groove exposes a large hydrophobic surface to aqueous milieu, making the cytosolic domain of the tail-anchored Bax less stable, thereby forcing a conformational change to bury the hydrophobic residues in the MOM, particularly those in the more
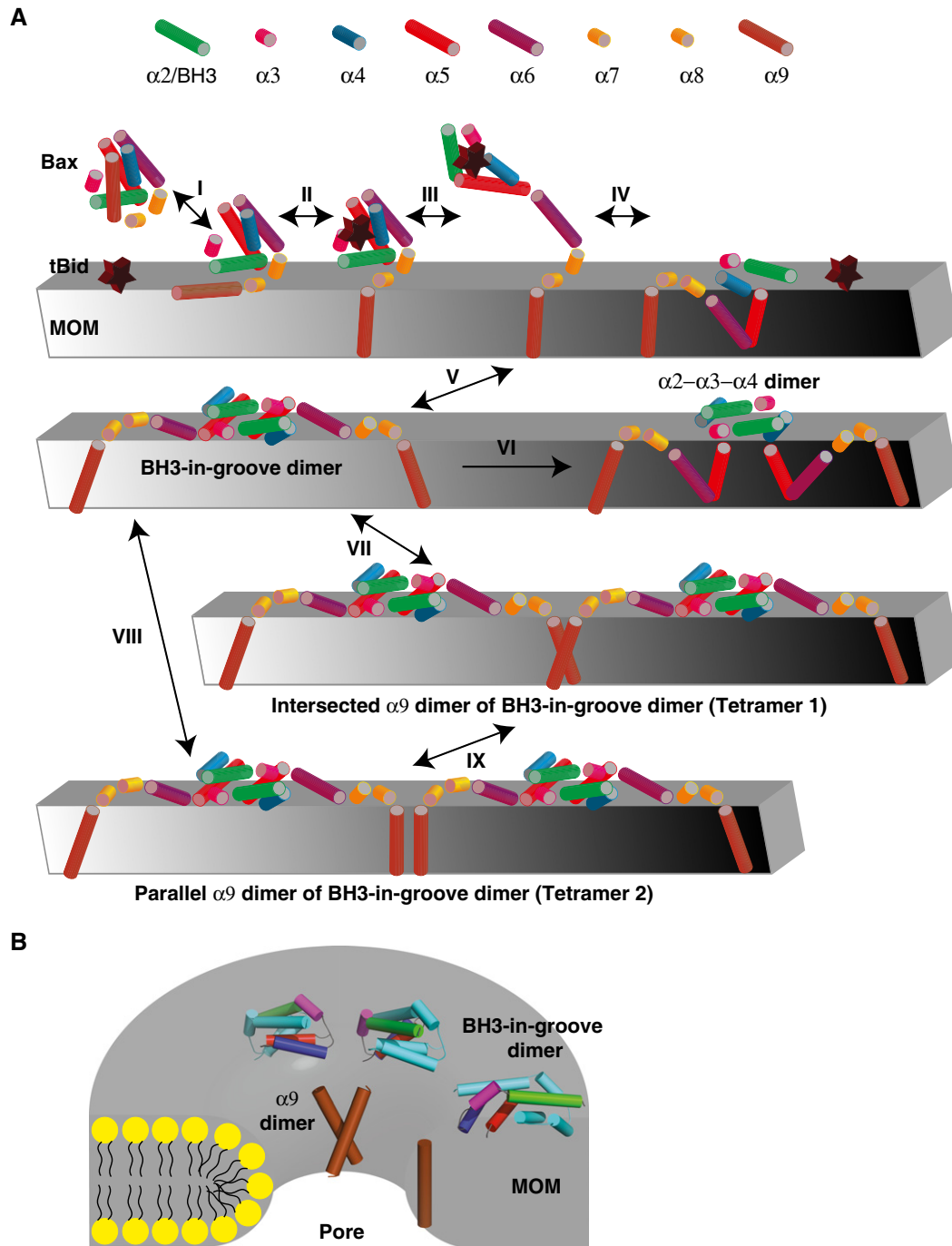
Figure 11. A model for conformational changes and interactions of Bax at the MOM, and the resulting pore.

A   Schematics illustrate the soluble Bax monomer and the MOM-bound Bax monomers, dimers and tetramers. The helices α2-α9 are depicted as cylinders with the indicated colors, and the helix α1 is omitted for simplicity. The MOM-bound tBid, depicted as a star, enhances cytosolic Bax interaction with the membrane (step I) and binds to the groove of Bax, thereby releasing α9 from the groove to the membrane (step II). The tBid binding also unfolds the Bax separating the latch (α6-α8) from the core (α2-α5) (step III). After tBid dissociates, the activated Bax monomer either embeds more hydrophobic regions such as α5 and α6 into the membrane (step IV) or binds other activated Bax monomer forming a BH3-in-groove dimer on the membrane surface (step V). After α5 is released into the membrane, the remnant BH3-in-groove dimer is rearranged to a α2-α3-α4 dimer (step VI). A Bax tetramer is then formed by two BH3-in-groove dimers via an additional dimer interface formed by two membrane-embedded α9 helices either intersected (step VII) or in parallel (step VIII). These Bax complexes may be in equilibrium with one another, but the BH3-in-groove dimerization is a prerequisite for the other dimerizations. In principle, combinations of these dimer interfaces would be sufficient to generate higher order oligomers, although other dimer interfaces have been discovered.

B   A lipidic pore in the MOM is illustrated with BH3-in-groove dimers located on the cytosolic surface of the membrane and α9 monomer and dimer at the rim. Note that the BH3-in-groove dimers are partially embedded in the cytosolic monolayer, generating membrane tension that induces the pore, while the α9 monomer and dimer are integrated into the highly curved monolayer to reduce the line tension, thereby stabilizing and expanding the pore.

hydrophobic α5 and those on the hydrophobic side of the amphipathic α2 (Fig 2). Consistently, our previous study suggested that the mitochondrial Bax monomer could embed α5, α6, and α9 in the MOM before oligomerization (Annis *et al*, 2005). A recent study also showed that the S184L mutation in α9 inserted not only α9 but also α5 and α6 into the MOM in the absence of tBid (Westphal *et al*, 2014a). Alternatively, α9 could be released from the membrane and reoccupy the empty groove, thereby refolding the Bax monomer, which could then return to the cytosol through retrotranslocation, a cellular process regulated by both anti- and pro-apoptotic family members (Billen *et al*, 2008; Edlich *et al*, 2011; Schellenberg *et al*, 2013; Todt *et al*, 2013, 2015). The G108E mutation adds a strong hydrogen donor to the edge of the groove, which increases the propensity for hydrogen bonding with the α9 residues in vicinity, and hence could stabilize the α9 in the groove, thereby keeping Bax soluble in the cytosol (Suzuki *et al*, 2000). The S184V mutation apparently overwrites the inhibitory effect of G108E on the mitochondrial targeting reactivating the MOMP and apoptotic activity (Figs 9 and EV2) (Kim *et al*, 2009). In the absence of membranes, a domain-swapped Bax dimerization could bury some of these hydrophobic residues as shown by the crystal structure of BaxΔα9 dimer (Czabotar *et al*, 2013). However, such dimerization would unlikely to occur in cells because activation of Bax takes place at membranes (Lovell *et al*, 2008), and the domain-swapped BaxΔα9 dimer is a detergent-induced complex that does not form by active Bax at membranes, as demonstrated in a recent DEER study (Bleicken *et al*, 2014). Here, we also saw majority of the Bax dimerizations in the mitochondrial, but not the soluble fraction (Figs EV3E, EV4D, and EV5D).

The BH3-in-groove dimer interface is formed by two tail-anchored Bax proteins (step V) after departure of the BH3 activator from the groove that readies both the BH3 region and the groove of Bax for their engagement (Fig 1). The crystal structure of tBid BH3 peptide in complex with the domain-swapped BaxΔα9 dimer displays a cavity in the BH3-binding groove (Czabotar *et al*, 2013) that may destabilize the complex, thereby facilitating the departure of tBid BH3 peptide and the exposure of Bax BH3 region. This complex structure also shows separation of the latch (α6-α8) from the core (α1-α5) of Bax, implying that the binding of tBid BH3 peptide to Bax groove induces the separation (step III). This "unlatching" event would occur before the BH3-in-groove dimerization required for Bax function (Figs 4 and 9), because disulfide linkage of α5 and α6 blocked tBid-induced MOMP by Bax (Czabotar *et al*, 2013), and opening of the α5-α6 hairpin in membrane-bound Bax is consistent with a DEER-derived distance between the spin pair located at the beginning and the end of the hairpin (Bleicken *et al*, 2014). The core–latch separation was also observed through FRET imaging in apoptotic cells (Gahl *et al*, 2014).

The BH3-in-groove dimerization exposes the hydrophobic residues in α4 and α5 to aqueous milieu (Czabotar *et al*, 2013), but only transiently because this high energetic state is quickly relaxed to a low energetic one either by burial of these hydrophobic residues in the cytosolic leaflet of the MOM bilayer (step V) or by release of the more hydrophobic α5, a part of the groove that houses the BH3 region, into the membrane (step VI; Fig 2). In contrast, the more amphipathic α4 does not insert into the membrane. Instead, α4 adjusts its position in the remnant dimer to form a α2-α3-α4 dimer on the membrane to hide some of the hydrophobic residues from

aqueous milieu (step VI; Figs 2 and 3). These conformational changes would separate α4 from α5, an implication somewhat different than that from the crystallography study, which concluded that α4 and α5 were not separated in the activated mitochondrial Bax (Czabotar *et al*, 2013). Most likely, α4 and α5 become separated in a fraction of, but not all, Bax proteins when they are activated and bound to mitochondria.

After the departure of α5, the remnant BH3-in-groove dimer rearranges to the helices α2-α3-α4 dimer (step VI), in which the α2 and α3 from one Bax are merged into a single helix that forms an antiparallel coiled-coil dimer on the membrane with its counterpart from the other Bax (Fig 3). This rearrangement re-stabilizes this dimer interface on the MOM by shielding the hydrophobic residues either in the new interface or in the cytosolic leaflet of the bilayer. It is conceivable that the α2-α3-α4 dimer could be formed directly by the Bax monomer that has the α5, α6, and α9 embedded in the MOM, but the α2, α3, and α4 exposed to the cytosol (step IV product) and hence available for dimerization. However, inhibition of the α2-α3-α4 dimerization by the G108E mutation that should not directly disrupt the α2-α3-α4 dimer, but rather the BH3-in-groove dimer (Fig 4), suggests that the α2-α3-α4 dimerization depends on, and thus occurs downstream of, the BH3-in-groove dimerization. The MD simulation (Appendix Fig S4) indicates the α2-α3-α4 dimer structure we show here based on the static modeling represents a cohort of different, yet related, conformations that likely coexist among the membrane-bound Bax complexes.

The α9 from one BH3-in-groove dimer binds its counterpart from the other dimer (step VII and VIII), resulting in an intersected or parallel α9 dimer interface in the membrane (Figs 5 and 6). As shown by the G108E mutant (Fig 7C), the α9 dimerization also depends on the BH3-in-groove dimerization, hence occurring downstream, to link the BH3-in-groove dimers to tetramers and higher order oligomers (Fig 8).

Numerous studies suggest that active Bax embeds into the cytosolic monolayer to generate membrane tension that induces lipidic pore in the MOM bilayer (Basanez *et al*, 2002; Terrones *et al*, 2004; Schafer *et al*, 2009; Bleicken *et al*, 2013). The membrane tension is proportional to the local concentration of Bax that is increased initially by the BH3-in-groove dimerization and further by the α9 dimerization. The membrane tension is also proportional to the regions of Bax that can partition into the cytosolic monolayer, including α9, because α9 only has three helical turns embedded in the MOM (Fig 5), too short to span the entire bilayer. Once the lipidic pore is formed, α9 would slide into the rim, where the bilayer is fused to a highly curved monolayer. The α9 at the rim would reduce the line tension, stabilizing the lipidic pore. The α9 dimerization at the rim might recruit more Bax proteins to the vicinity, expanding the pore. Therefore, both membrane insertion and dimerization of α9 would induce, stabilize, and expand the lipidic pore. As shown by the G179I and T182I mutants (Figs 10 and EV5E), more α9 insertion and the consequently more BH3-in-groove dimerization could compensate for less α9 dimerization to enlarge the pore. However, at a normal α9 insertion level, we propose that α9 dimerization becomes critical to the pore expansion. Thus, dimerization of α9 is not required for the small pore formation that releases cytochrome c, but facilitates large pore formation that releases Smac and larger proteins. The membrane insertion of α5 may play a similar role as it also has three helical turns embedded

in the membrane (Fig 2), and thus prefers the highly curved mono-layer at the pore rim. In fact, α5 peptide can form a toroidal pore by localizing to the rim (Garcia-Saez *et al*, 2007; Qian *et al*, 2008), although α9 peptide can oligomerize in membranes and may form a barrel-stave proteinous pore (Garg *et al*, 2013).

We built a model to illustrate the architecture of Bax pore in the MOM (Fig 11B). In this model, the BH3-in-groove dimers are placed on the cytosolic surface of the MOM, forming the outer ring of the pore. The α9 dimers are placed at the edge of the bilayer, forming the rim of the pore with lipid head groups in the highly curved monolayer. The α9 dimer of BH3-in-groove dimer is one of the multiple tetrameric units that are assembled into an oligomer. The number of Bax molecules in the oligomer dictates the pore size. In order to transport hydrated cytochrome c across the MOM, the mini-mal pore diameter must be ~50 Å. This model represents one conformation of a dynamic Bax pore, variations from which are possible. For example, the α5 may leave the BH-in-groove dimer, inserting into the bilayer or joining the α9 at the pore rim, whereby the remnant of the dimer rearranges to the α2-α3-α4 dimer that remains on the cytosolic surface of the MOM.

The DEER study proposed another conformation for the pore (Bleicken *et al*, 2014), in which the BH3-in-groove dimer is located at the rim with the hydrophobic side of α4 and α5 embedded in the curved lipid monolayer, while the α9 is inserted into the bilayer farther from the rim and linked to the α5 by α6 located on the surface of the bilayer. Due to the symmetry of the BH3-in-groove dimer, this conformation requires two α6 helices, one from each monomer, to locate on the opposite surfaces of the MOM, and two α9 helices to span the MOM in an antiparallel orientation. While this model fits some of the intra- and intermolecular distances derived from the DEER data, the broad distance distribution indicates a dynamic localization of the α6 and α9 relative to the BH3-in-groove dimer that requires other models to fit. Moreover, it is difficult to imagine how a large part of the Bax molecule stretching from α6 to α9 can cross to the intermembrane space side from the cytosolic side of the MOM where the initial binding occurs to drive the pore formation (Andrews, 2014). Our model, on the other hand, would allow the BH3-in-groove dimer to slide into the rim after pore forma-tion, which might further stabilize and expand the lipidic pore. Moreover, while the localization of α6 on the MOM surface is supported by previous IASD-labeling studies (Annis *et al*, 2005; Westphal *et al*, 2014a), the transmembrane topology of α9 requires at least five helical turns to be buried in the bilayer, which is incon-sistent with our IASD-labeling data (Fig 5) unless α9 also accesses the aqueous interior of the pore or IASD can label the residues located in the bilayer but near the surfaces such as the lipid head group region. Finally, the antiparallel orientation of two α9 helices is at odds with our disulfide-crosslinking data (Fig 6) and others' intermolecular FRET imaging data (Gahl *et al*, 2014) that support a parallel or intersected α9 dimer model.

By monitoring the conformation and interaction of active Bax at mitochondria in a biologically relevant cell-free system supple-mented with a cell system, we have demonstrated the formation of two separate dimer interfaces. The BH3-in-groove interface located on the membrane surface is formed earlier than and required for the formation of the α9 interface inside the membrane. Together, both interfaces assemble Bax proteins into oligomers that induce membrane permeabilization by forming

lipidic pores. While it appears that the BH3-in-groove dimerization is required for pore formation, α9 dimerization may be primarily involved in pore expansion. The concerted action of this series of protein–protein interactions and the subsequent membrane desta-bilization results in the release of not only cytochrome c, which induces caspase activation, but also larger proteins like Smac, which neutralizes caspase inhibitors, thereby culminating in a full-scale apoptotic reaction that dismantles the cell. The protein complexes and conformations that we have characterized here may be potential targets for the future development of apoptotic modulators to eradicate cancer or to prevent ischemia reperfusion injury (Czabotar *et al*, 2014; Moldoveanu *et al*, 2014; Brahmbhatt *et al*, 2015).

Materials and Methods

Reagents

Single-cysteine Bax mutant plasmids for *in vitro* transcription and translation were constructed from pSPUTK vector (Stratagen) as described earlier (Ding *et al*, 2014). Additional mutations, as described in Results, were introduced into some of the single-cysteine mutants or wild-type Bax using QuickChange mutagenesis (Agilent technologies). The single-cysteine mutants were designated as a letter and a number that indicate the wild-type residue and its position follow by C that indicates the change to a cysteine. The other mutants were similarly designated. The single-cysteine tBid mutant pladmid was constructed from pSPUTK to include the same 5′ untranslated region as that in the Bax plasmid.

Human Bax protein with or without G179I or T182I mutation, and murine tBid protein were expressed and purified as described elsewhere (Zha *et al*, 2000; Yethon *et al*, 2003; Zhang *et al*, 2010). The Bax BH3 peptide was synthesized by Abgent as described in Tan *et al* (2006).

The rabbit polyclonal antibody to Bid (catalog No. ab77815) and the mouse monoclonal antibody to pyruvate dehydrogenase E1-alpha subunit (catalog No. ab110334) were from Abcam. The rabbit polyclonal antibody to Smac (catalog No. sc-22766) was from Santa Cruz Biotechnology. The rabbit polyclonal antibody to Bax and the sheep polyclonal antibody to cytochrome c were produced in David Andrews's laboratory.

MOMP assays

The ELISA-based cytochrome c release assay was performed as described earlier (Ding *et al*, 2014), except that we used 2 μl Bax protein synthesized in transcription/translation (TNT)-coupled SP6 RNA polymerase/reticulocyte lysate system (Promega), 17 nM puri-fied tBid protein, and 0.6 mg/ml Bax$^{-/-}$/Bak$^{-/-}$ mitochondria.

The immunoblot-based cytochrome c and Smac release assay began with incubation of 60 or 120 nM purified Bax protein with 1 mg/ml Bax$^{-/-}$/Bak$^{-/-}$ mitochondria in the absence or presence of 17 nM purified tBid protein at 37°C for 2 h. The resulting sample was centrifuged at 13,000 g and 4°C for 5 min. The supernatant and pellet were separated and analyzed by reducing SDS–PAGE and immunoblotting with the antibody to cytochrome c (dilution 1:1,500) or to Smac (dilution 1:750).

The fluorescence-based Smac-mCherry release assay was performed as described in Shamas-Din *et al* (2014) with 10, 20, or 40 nM purified Bax protein, and where indicated, 2 nM purified caspase-cleaved Bid protein (cBid).

Live cell imaging and analysis

Bax/Bak double-knockout (DKO) baby mouse kidney (BMK) cells were cultured in DMEM supplemented with 10% FBS. For transfections, Bax/Bak DKO cells were seeded at 1,000 cells/well in a 384-well imaging plate (PerkinElmer Cell Carrier Ultra) and transiently transfected 24 h later with Venus-Bax constructs (ratio of 1:6 DNA:Fugene HD transfection reagent from Promega). Cells were incubated for 14 h post-transfection of Venus-Bax constructs and then treated with or without 50 nM staurosporine (STS) for 8 h. Cells were stained 30 min prior to imaging with 5 µM Draq5 (BioStatus) and either 10 nM TMRE (Invitrogen) for activity assays or 100 nM Mitotracker Red (ThermoFischer) for colocalization studies. Cells were imaged using the Opera high-content screening system (PerkinElmer) with either a 20× air objective (for activity assays) or a 40× water immersion objective (for colocalization studies). Three channels were captured: Draq5, Venus, and TMRE or Mitotracker Red. Images were analyzed as in Shamas-Din *et al* (2013). Briefly, a script written for Acapella high-content imaging and analysis software (available for download from dwalab.ca) was used to segment and detect only Venus-positive cells. The same script was used to extract intensity and morphology features for each segmented cell as well as Pearson's correlation coefficient (for colocalization experiments). Dead cells were classified as small rounded up TMRE-negative cells. The percentage of apoptosis was calculated by taking total number of Venus-positive cells classified as dead and dividing by the total number of Venus-positive cells.

To minimize the effects of subjective bias in sample allocation and result analysis, a fully automated microscope was used to image cells based on a predetermined pattern of locations within the wells of an imaging plate. Therefore, the selection of cells analyzed was unbiased. Images acquired by the automated microscope were then analyzed numerically based on automated image analysis of computer-measured features in the images rather than a subjective interpretation.

Justifications for the statistical test used are that points are generally averages of ~150 randomly selected automatically analyzed cell images from three biological replicates. Standard deviation is reported to provide error bars on the histograms. However, to determine significance of differences between mutants, one-way ANOVA was used and determined that the means are not identical. *Post-hoc* multiple comparisons were made using a *t*-test with a *P*-value < 0.05 being significant. To correct for type I error, the Bonferroni correction was applied to the *P*-value (0.05/24(number of measurements)), and any *P*-value < 0.002083 is deemed significant. For expression levels, *post-hoc* multiple comparisons were made using a *t*-test with a *P*-value < 0.05 being significant. To correct for type I error, the Bonferroni correction was applied to the *P*-value (0.05/12 (number of measurements)), and any *P*-value < 0.00417 is deemed significant. *t*-tests were used to compare the Venus intensity of each mutant construct to that of WT Bax in order to compare expression levels. Raw data are plotted and means were compared to medians.

Data is close enough to normal distribution that standard deviation is a reasonable estimate.

Disulfide crosslinking

Disulfide crosslinking of mitochondria-bound Bax proteins was performed and analyzed as described in Ding *et al* (2014) with the following modifications. We incubated 15 µl *in vitro* synthesized [^{35}S]Met-labeled Bax protein, 17 µM Bax BH3 peptide, and 0.6 mg/ml Bax$^{-/-}$/Bak$^{-/-}$ mitochondria at 37°C for 1 h. The mitochondria with activated Bax were pelleted by centrifugation at 13,000 g and 4°C for 5 min. The mitochondria were resuspended in high salt buffer (400 mM KOAc, 4 mM Mg(OAc)$_2$, and 25 mM HEPES, pH 7.5) to remove loosely bound proteins before adding redox catalyst CuPhe to induce disulfide crosslinking. For some of the mitochondrial samples, low salt buffer (110 mM KOAc, 1 mM Mg(OAc)$_2$, and 25 mM HEPES, pH 7.5) was used, and the crosslinking results were similar to the "high salt" controls. The disulfide-crosslinked samples were precipitated by Cl$_3$CCOOH. The resulting protein pellets were resuspended in quenching buffer (20 mM N-ethylmaleimide (NEM), 100 mM EDTA, 1 mM NaAsO$_2$), solubilized in non-reducing SDS sample buffer (12.5% SDS, 500 mM Tris, 25% glycerol, 250 mM EDTA, and a trace of bromophenol blue) at 65°C for 30 min, and analyzed using SDS–15% PAGE and phosphorimaging.

Some of the disulfide-crosslinked samples were treated with Na$_2$CO$_3$ (pH 11.5) as described earlier (Billen *et al*, 2008), except that DTT was omitted from the 200-mM Na$_2$CO$_3$ solution and 0.5-M sucrose cushion. The resulting pellet and supernatant fractions were analyzed by SDS–PAGE and phosphorimaging as describe above, or by immunoblotting with mouse monoclonal antibody to pyruvate dehydrogenase E1-alpha subunit (dilution 1:2,500).

Immunoprecipitation

To identify the disulfide-linked products from the reactions containing single-cysteine Bax and tBid mutants, the samples were divided into two equal portions, and diluted approximately 1:7 in IP buffer containing 100 mM Tris pH 8.0, 100 mM NaCl, 10 mM EDTA, 1 mM PMSF, 1% (v/v) Triton X-100 and incubated with Bax (dilution 1:100) or Bid (dilution 1:1,600) antibody. Reactions were rotated overnight at 4°C. The resulting immuno-complexes were bound to Sepharose protein G beads (6–8 µl of 50% bead suspension in IP buffer) for 2 h at 4°C. After centrifugation at 2,000 *g* for 30 s at 4°C, the beads were washed three times with IP buffer and twice with 100 mM Tris pH 8.0 and 100 mM NaCl. The bound proteins were eluted from the beads with non-reducing SDS sample buffer and analyzed by non-reducing SDS–PAGE and phosphorimaging.

4-acetamido-4′-((iodoacetyl)amino)stilbene-2,2′-disulfonic acid (IASD) labeling

IASD labeling of mitochondria-bound Bax proteins was performed and analyzed as described in Ding *et al* (2014) with the following modifications. We incubated 2.5 µl Bax protein synthesized *in vitro* with 17 µM Bax BH3 peptide or 17 nM tBid protein, and 0.8 mg/ml Bax$^{-/-}$/Bak$^{-/-}$ mitochondria at 37°C for 1 h. The mitochondria with activated Bax were pelleted by centrifugation as described above, and resuspended in medium salt buffer (200 mM KOAc,

2 mM Mg(OAc)$_2$, and 10 mM HEPES, pH 7.5) to increase IASD-labeling efficiency (Westphal *et al*, 2014a). For some mitochondrial samples, low salt buffer was used, and the IASD-labeling results were similar to the "medium salt" controls. The mitochondrial suspension was split equally to five, and 0.5 mM IASD was added to each aliquot alongside 230 mM Tris–HCl, pH 7.5, 100 ng/ml each of leupeptin, antipain, chymostatin, and pepstatin, 150 ng/ml aprotinin, 0.05 mM DTT, and, if indicated, 2% 3-((3-cholamidopropyl) dimethylammonio)-1-propanesulfonate (CHAPS), 4 M urea, or both. The labeling reactions were carried out in dark at 22°C for 30 min and then quenched by 50 mM 2-mercaptoethanol. For the "0 min" labeling control, 2-mercaptoethanol was added prior to the addition of IASD to prevent the labeling. After the concentration of CHAPS and urea in each sample was brought to 2% and 4 M, respectively, the proteins were precipitated by Cl$_3$CCOOH.

For reducing SDS-gradient (15–16%) PAGE analysis, the protein pellet was solubilized at 65°C for 30 min in the SDS sample buffer plus 1 M 2-mercaptoethanol. For IEF analysis, the protein pellet was sonicated at 22°C for 20 min in IEF sample buffer (10 mM Tris–HCl, pH 7.5, 8 M urea, 4% CHAPS, 4% Tergitol NP-40, 0.4% Triton X-100, 30% glycerol, 2% 5–8 ampholyte, 1 M 2-mercaptoethanol, and a trace of bromophenol blue), loaded on a pH 5–8 gel (1.5% 5–8 ampholyte, 0.5% 3–10 ampholyte, 7% acrylamide (acrylamide: methylenebisacrylamide = 37.5:1), 7 M urea, 2% CHAPS, 4% Tergitol NP-40, 0.08% tetramethylethylenediamine, and 0.09% ammonium persulfate, pre-run at 100 V for 30 min), and run with anode buffer (50 mM H$_3$PO$_4$, pH ~4) and cathode buffer (20 mM lysine, 20 mM arginine, pH ~10) at 100 V for 1 h, 250 V for 1.5 h, and 400 V for 14 h 45 min. The radioactive proteins in the resulting gels were detected by phosphorimaging, and quantified using Multi Gauge program (Fujifilm) as described in Appendix Fig S3A.

Computational modeling of Bax dimer interfaces

α2-α3-α4 dimer interface
We modeled this dimer based on the published structure of Bax monomer (PDB entry: 1F16) and the distance restraints provided by the disulfide crosslinking between the specific interfacial residues after they were replaced by cysteines (Fig 3A). Briefly, the partial Bax structure formed by residues 54–103 including α2, α3, and α4 helices and the inter-helical loops were extracted from the whole structure. The loops were removed and a global search was performed to optimize the distance restraints and the protein geometry according to the following procedures.

First, helices α2 (residues 54–71), α3 (residues 75–81), and α4 (residues 88–99) were converted to poly-alanine and allowed to independently move in space as rigid bodies, using a Monte Carlo procedure to minimize the energy of springs functions introduced to represent the linkages from crosslinking experiments. The springs were places between the Cβ atoms of each crosslinked position in the two chains (S55-R94′, L59-L76′, S62-S72′, and E69-E69′) using a spring constant of 200 kcal/mol/Å^2 and an energy minimum distance of 5 Å. Spring penalties were not calculated for distances of the crosslinked Cβ atoms below 5 Å. In addition, the helical termini of α2 and α3, and of α3 and α4 were also constrained to remain within 6 Å of distance. Once these distance constraints were minimized, the original side chains were reintroduced and the same procedure was continued—except that each cycle included a round

of side chain optimization—until the energy converged. The α2, α3, and α4 helices were then connected together by the residues with favorable geometry using fragments extracted from the PDB database according to a procedure previously described (LaPointe *et al*, 2013). Briefly, protein fragments with pattern $hhha_xhhh$ were extracted from high-resolution X-ray structures, where h are positions in a helical conformation and a_x are positions in any conformation corresponding to the number needed for the loop connecting the helices ($x = 3$ for α2-α3 loop; $x = 6$ for the α3-α4 loop). The termini of the inter-helical fragments were then aligned with the termini of the helices to be connected to obtain favorable geometries and the helices and fragments were fused. Only the N, C, CA, and O atoms were considered for the alignment and the fragments with the lowest root-mean-square deviation (RMSD) were selected. The side chains on the fragment were replaced with the one corresponding to the native Bax sequence and their conformation was optimized.

The procedure yielded a well-packed model with favorable energies, in which a distorted helical region connected helices α2 and α3. To investigate whether the geometry of the α2-α3 region was compatible with canonical helical conformation, the procedure was repeated as described except that helices α2 and α3 were fused into a single canonical helical fragment. This second computation produced a model closely related to the original that satisfied the distance constraints in similar fashion but had slightly lower energies. This model is illustrated in Fig 3D.

In the procedure, the energies were calculated using the CHARMM 22 van der Waals' function (MacKerell *et al*, 1998) and the hydrogen bonding function of SCWRL 4 (Krivov *et al*, 2009), as implemented in MSL C++ libraries (Kulp *et al*, 2012). All side chain optimization procedures were performed using the Energy-Based Conformer Library applied at the 95% level (Subramaniam & Senes, 2012, 2014) with a greedy trials algorithm (Xiang & Honig, 2001) as implemented in MSL.

α9 dimer interface
Two models were predicted for the membrane-embedded α9 dimer. The first model was predicted *ab initio* by CATM program (Mueller *et al*, 2014) from the sequence of α9, G^{166}TP^{168}TWQTVTIFVAGVL-TASLTIWKKM^{191}, except that Pro^{168} was replaced by alanine to increase the helical propensity. The program predicted a homo-dimeric structure adopting a GASright conformation (Walters & DeGrado, 2006) mediated by the GxxxA sequence motif (Russ & Engelman, 2000; Senes *et al*, 2000). The resulting intersected α9 dimer model (Fig 6A) fits the disulfide-crosslinking data from four single-cysteine Bax mutants (Fig 6B).

The second model (the parallel α9 dimer) was obtained through a systematic search of the dimer conformational space directed by the disulfide-crosslinking data from the other four single-cysteine Bax mutants (Fig 6D). The search program generated two standard helices for α9 and performed a systematic search of the space of all possible C2 symmetrical dimer geometries, varying four degrees of freedom, (i) the rotation around the helical axis, (ii) the inter-helical crossing angle, (iii) the position of crossing point along the axis of symmetry, and (iv) the inter-helical distance. The distance between the β-carbon atoms of Q171, A178, T182, and L185 was evaluated for each geometry. If all four distances fell below a 6 Å, the side chains were optimized. The energy of association of this optimized dimer was computed as the difference between the energy of the

dimer and the energy of a side chain optimized monomer, and all dimers with a favorable energy of association were stored. From this set of structures, a structure with good packing was selected by visual inspection (Fig 6F).

Disruptive mutations were predicted from both α9 dimer models by a computational mutagenesis protocol. Each position was mutated into glycine, alanine, leucine, valine, isoleucine, and phenyl-alanine residues. For each mutation, side chains were optimized and the energy of association was computed for the dimer using hydrogen bonding and van der Waals' functions as reported previously (LaPointe *et al*, 2013). Each mutation was classified into one of four categories based on the difference in the energy (ΔE) between the wild-type and the mutated dimer. The classification is as follows: (i) silent: $\Delta E \leq 2$ units, (ii) significant: $2 < \Delta E \leq 4$ units, (iii) mildly disruptive: $4 < \Delta E \leq 8$ units, and (iv) disruptive: $\Delta E > 8$ units. An average score was computed for each position, and used to identify disruptive mutations. All programs were implemented using the MSL molecular modeling software library (Kulp *et al*, 2012).

Molecular dynamics simulations

See Appendix Supplementary Methods.

Expanded View for this article is available online.

Acknowledgements

Author contributions

JLin and DWA conceptualized the study, designed experiments, analyzed data, and wrote the paper. ZZ, JK, HB, SML, JD, and FH conducted experiments and analyzed data. SS, BH, SGFC, FAH, XCZ, and AS performed computational modeling and edited the paper. CL and JLi performed molecular dynamics simulations and edited the paper.

Conflict of interest

The authors declare that they have no conflict of interest.

References

Aluvila S, Mandal T, Hustedt E, Fajer P, Choe JY, Oh KJ (2014) Organization of the mitochondrial apoptotic BAK pore: oligomerization of the BAK homodimers. *J Biol Chem* 289: 2537–2551

Andrews DW (2014) Pores of no return. *Mol Cell* 56: 465–466

Annis MG, Soucie EL, Dlugosz PJ, Cruz-Aguado JA, Penn LZ, Leber B, Andrews DW (2005) Bax forms multispanning monomers that oligomerize to permeabilize membranes during apoptosis. *EMBO J* 24: 2096–2103

Basanez G, Sharpe JC, Galanis J, Brandt TB, Hardwick JM, Zimmerberg J (2002) Bax-type apoptotic proteins porate pure lipid bilayers through a mechanism sensitive to intrinsic monolayer curvature. *J Biol Chem* 277: 49360–49365

Billen LP, Kokoski CL, Lovell JF, Leber B, Andrews DW (2008) Bcl-XL inhibits membrane permeabilization by competing with Bax. *PLoS Biol* 6: e147

Bleicken S, Classen M, Padmavathi PV, Ishikawa T, Zeth K, Steinhoff HJ, Bordignon E (2010) Molecular details of Bax activation, oligomerization, and membrane insertion. *J Biol Chem* 285: 6636–6647

Bleicken S, Landeta O, Landajuela A, Basanez G, Garcia-Saez AJ (2013) Proapoptotic Bax and Bak proteins form stable protein-permeable pores of tunable size. *J Biol Chem* 288: 33241–33252

Bleicken S, Jeschke G, Stegmueller C, Salvador-Gallego R, Garcia-Saez AJ, Bordignon E (2014) Structural model of active bax at the membrane. *Mol Cell* 56: 496–505

Borner C, Andrews DW (2014) The apoptotic pore on mitochondria: are we breaking through or still stuck? *Cell Death Differ* 21: 187–191

Brahmbhatt H, Oppermann S, Osterlund EJ, Leber B, Andrews DW (2015) Molecular pathways: leveraging the BCL-2 interactome to kill cancer cells-mitochondrial outer membrane permeabilization and beyond. *Clin Cancer Res* 21: 2671–2676

Chai J, Du C, Wu JW, Kyin S, Wang X, Shi Y (2000) Structural and biochemical basis of apoptotic activation by Smac/DIABLO. *Nature* 406: 855–862

Chi X, Kale J, Leber B, Andrews DW (2014) Regulating cell death at, on, and in membranes. *Biochim Biophys Acta* 1843: 2100–2113

Czabotar PE, Lee EF, Thompson GV, Wardak AZ, Fairlie WD, Colman PM (2011) Mutation to Bax beyond the BH3 domain disrupts interactions with pro-survival proteins and promotes apoptosis. *J Biol Chem* 286: 7123–7131

Czabotar PE, Westphal D, Dewson G, Ma S, Hockings C, Fairlie WD, Lee EF, Yao S, Robin AY, Smith BJ, Huang DC, Kluck RM, Adams JM, Colman PM (2013) Bax crystal structures reveal how BH3 domains activate bax and nucleate its oligomerization to induce apoptosis. *Cell* 152: 519–531

Czabotar PE, Lessene G, Strasser A, Adams JM (2014) Control of apoptosis by the BCL-2 protein family: implications for physiology and therapy. *Nat Rev Mol Cell Biol* 15: 49–63

Dewson G, Ma S, Frederick P, Hockings C, Tan I, Kratina T, Kluck RM (2012) Bax dimerizes via a symmetric BH3:groove interface during apoptosis. *Cell Death Differ* 19: 661–670

Ding J, Mooers BH, Zhang Z, Kale J, Falcone D, McNichol J, Huang B, Zhang XC, Xing C, Andrews DW, Lin J (2014) After embedding in membranes antiapoptotic Bcl-XL protein binds both Bcl-2 homology region 3 and helix 1 of proapoptotic Bax protein to inhibit apoptotic mitochondrial permeabilization. *J Biol Chem* 289: 11873–11896

Du C, Fang M, Li Y, Li L, Wang X (2000) Smac, a mitochondrial protein that promotes cytochrome c-dependent caspase activation by eliminating IAP inhibition. *Cell* 102: 33–42

Edlich F, Banerjee S, Suzuki M, Cleland MM, Arnoult D, Wang C, Neutzner A, Tjandra N, Youle RJ (2011) Bcl-x(L) retrotranslocates Bax from the mitochondria into the cytosol. *Cell* 145: 104–116

Gahl RF, He Y, Yu S, Tjandra N (2014) Conformational rearrangements in the pro-apoptotic protein, Bax, as it inserts into mitochondria: a cellular death switch. *J Biol Chem* 289: 32871–32882

Garcia-Saez AJ, Chiantia S, Salgado J, Schwille P (2007) Pore formation by a Bax-derived peptide: effect on the line tension of the membrane probed by AFM. *Biophys J* 93: 103–112

Garcia-Saez AJ (2012) The secrets of the Bcl-2 family. *Cell Death Differ* 19: 1733–1740

Garg P, Nemec KN, Khaled AR, Tatulian SA (2013) Transmembrane pore formation by the carboxyl terminus of Bax protein. *Biochim Biophys Acta* 1828: 732–742

Gavathiotis E, Reyna DE, Davis ML, Bird GH, Walensky LD (2010) BH3-triggered structural reorganization drives the activation of proapoptotic BAX. *Mol Cell* 40: 481–492

Iyer S, Bell F, Westphal D, Anwari K, Gulbis J, Smith BJ, Dewson G, Kluck RM (2015) Bak apoptotic pores involve a flexible C-terminal region and juxtaposition of the C-terminal transmembrane domains. *Cell Death Differ* 22: 1665–1675

Kim H, Tu HC, Ren D, Takeuchi O, Jeffers JR, Zambetti GP, Hsieh JJ, Cheng EH (2009) Stepwise activation of BAX and BAK by tBID, BIM, and PUMA initiates mitochondrial apoptosis. *Mol Cell* 36: 487–499

Krivov GG, Shapovalov MV, Dunbrack RL Jr (2009) Improved prediction of protein side-chain conformations with SCWRL4. *Proteins* 77: 778–795

Kulp DW, Subramaniam S, Donald JE, Hannigan BT, Mueller BK, Grigoryan G, Senes A (2012) Structural informatics, modeling, and design with an open-source Molecular Software Library (MSL). *J Comput Chem* 33: 1645–1661

Kuwana T, Mackey MR, Perkins G, Ellisman MH, Latterich M, Schneiter R, Green DR, Newmeyer DD (2002) Bid, Bax, and lipids cooperate to form supramolecular openings in the outer mitochondrial membrane. *Cell* 111: 331–342

LaPointe LM, Taylor KC, Subramaniam S, Khadria A, Rayment I, Senes A (2013) Structural organization of FtsB, a transmembrane protein of the bacterial divisome. *Biochemistry* 52: 2574–2585

Liu Z, Lin H, Ye S, Liu QY, Meng Z, Zhang CM, Xia Y, Margoliash E, Rao Z, Liu XJ (2006) Remarkably high activities of testicular cytochrome c in destroying reactive oxygen species and in triggering apoptosis. *Proc Natl Acad Sci USA* 103: 8965–8970

Lovell JF, Billen LP, Bindner S, Shamas-Din A, Fradin C, Leber B, Andrews DW (2008) Membrane binding by tBid initiates an ordered series of events culminating in membrane permeabilization by Bax. *Cell* 135: 1074–1084

Lucken-Ardjomande S, Montessuit S, Martinou JC (2008) Contributions to Bax insertion and oligomerization of lipids of the mitochondrial outer membrane. *Cell Death Differ* 15: 929–937

MacKenzie KR, Prestegard JH, Engelman DM (1997) A transmembrane helix dimer: structure and implications. *Science* 276: 131–133

MacKerell AD, Bashford D, Bellott M, Dunbrack RL, Evanseck JD, Field MJ, Fischer S, Gao J, Guo H, Ha S, Joseph-McCarthy D, Kuchnir L, Kuczera K, Lau FT, Mattos C, Michnick S, Ngo T, Nguyen DT, Prodhom B, Reiher WE *et al* (1998) All-atom empirical potential for molecular modeling and dynamics studies of proteins. *J Phys Chem B* 102: 3586–3616

Moldoveanu T, Follis AV, Kriwacki RW, Green DR (2014) Many players in BCL-2 family affairs. *Trends Biochem Sci* 39: 101–111

Mueller BK, Subramaniam S, Senes A (2014) A frequent, GxxxG-mediated, transmembrane association motif is optimized for the formation of interhelical Calpha-H hydrogen bonds. *Proc Natl Acad Sci USA* 111: E888–E895

Ormo M, Cubitt AB, Kallio K, Gross LA, Tsien RY, Remington SJ (1996) Crystal structure of the Aequorea victoria green fluorescent protein. *Science* 273: 1392–1395

Qian S, Wang W, Yang L, Huang HW (2008) Structure of transmembrane pore induced by Bax-derived peptide: evidence for lipidic pores. *Proc Natl Acad Sci USA* 105: 17379–17383

Russ WP, Engelman DM (2000) The GxxxG motif: a framework for transmembrane helix-helix association. *J Mol Biol* 296: 911–919

Schafer B, Quispe J, Choudhary V, Chipuk JE, Ajero TG, Du H, Schneiter R, Kuwana T (2009) Mitochondrial outer membrane proteins assist Bid in Bax-mediated lipidic pore formation. *Mol Biol Cell* 20: 2276–2285

Schellenberg B, Wang P, Keeble JA, Rodriguez-Enriquez R, Walker S, Owens TW, Foster F, Tanianis-Hughes J, Brennan K, Streuli CH, Gilmore AP (2013) Bax exists in a dynamic equilibrium between the cytosol and mitochondria to control apoptotic priming. *Mol Cell* 49: 959–971

Senes A, Gerstein M, Engelman DM (2000) Statistical analysis of amino acid patterns in transmembrane helices: the GxxxG motif occurs frequently and in association with beta-branched residues at neighboring positions. *J Mol Biol* 296: 921–936

Shamas-Din A, Bindner S, Zhu W, Zaltsman Y, Campbell C, Gross A, Leber B, Andrews DW, Fradin C (2013) tBid undergoes multiple conformational changes at the membrane required for Bax activation. *J Biol Chem* 288: 22111–22127

Shamas-Din A, Satsoura D, Khan O, Zhu W, Leber B, Fradin C, Andrews DW (2014) Multiple partners can kiss-and-run: Bax transfers between multiple membranes and permeabilizes those primed by tBid. *Cell Death Dis* 5: e1277

Shamas-Din A, Bindner S, Chi X, Leber B, Andrews DW, Fradin C (2015) Distinct lipid effects on tBid and Bim activation of membrane permeabilization by pro-apoptotic Bax. *Biochem J* 467: 495–505

Subramaniam S, Senes A (2012) An energy-based conformer library for side chain optimization: improved prediction and adjustable sampling. *Proteins* 80: 2218–2234

Subramaniam S, Senes A (2014) Backbone dependency further improves side chain prediction efficiency in the Energy-based Conformer Library (bEBL). *Proteins* 82: 3177–3187

Sulistijo ES, Mackenzie KR (2009) Structural basis for dimerization of the BNIP3 transmembrane domain. *Biochemistry* 48: 5106–5120

Suzuki M, Youle RJ, Tjandra N (2000) Structure of Bax: coregulation of dimer formation and intracellular localization. *Cell* 103: 645–654

Tan C, Dlugosz PJ, Peng J, Zhang Z, Lapolla SM, Plafker SM, Andrews DW, Lin J (2006) Auto-activation of the apoptosis protein Bax increases mitochondrial membrane permeability and is inhibited by Bcl-2. *J Biol Chem* 281: 14764–14775

Terrones O, Antonsson B, Yamaguchi H, Wang HG, Liu J, Lee RM, Herrmann A, Basanez G (2004) Lipidic pore formation by the concerted action of proapoptotic BAX and tBID. *J Biol Chem* 279: 30081–30091

Todt F, Cakir Z, Reichenbach F, Youle RJ, Edlich F (2013) The C-terminal helix of Bcl-x(L) mediates Bax retrotranslocation from the mitochondria. *Cell Death Differ* 20: 333–342

Todt F, Cakir Z, Reichenbach F, Emschermann F, Lauterwasser J, Kaiser A, Ichim G, Tait SW, Frank S, Langer HF, Edlich F (2015) Differential retrotranslocation of mitochondrial Bax and Bak. *EMBO J* 34: 67–80

Verhagen AM, Ekert PG, Pakusch M, Silke J, Connolly LM, Reid GE, Moritz RL, Sompson RJ, Vaux DL (2000) Identification of DIABLO, a mammalian protein that promotes apoptosis by binding to and antagonizing IAP proteins. *Cell* 102: 43–53

Volkmann N, Marassi FM, Newmeyer DD, Hanein D (2014) The rheostat in the membrane: BCL-2 family proteins and apoptosis. *Cell Death Differ* 21: 206–215

Walters RF, DeGrado WF (2006) Helix-packing motifs in membrane proteins. *Proc Natl Acad Sci USA* 103: 13658–13663

Westphal D, Dewson G, Menard M, Frederick P, Iyer S, Bartolo R, Gibson L, Czabotar PE, Smith BJ, Adams JM, Kluck RM (2014a) Apoptotic pore formation is associated with in-plane insertion of Bak or Bax central

helices into the mitochondrial outer membrane. *Proc Natl Acad Sci USA* 111: E4076 – E4085

Westphal D, Kluck RM, Dewson G (2014b) Building blocks of the apoptotic pore: how Bax and Bak are activated and oligomerize during apoptosis. *Cell Death Differ* 21: 196 – 205

Xiang Z, Honig B (2001) Extending the accuracy limits of prediction for side-chain conformations. *J Mol Biol* 311: 421 – 430

Yamaguchi R, Andreyev A, Murphy AN, Perkins GA, Ellisman MH, Newmeyer DD (2007) Mitochondria frozen with trehalose retain a number of biological functions and preserve outer membrane integrity. *Cell Death Differ* 14: 616 – 624

Yethon JA, Epand RF, Leber B, Epand RM, Andrews DW (2003) Interaction with a membrane surface triggers a reversible conformational change in Bax normally associated with induction of apoptosis. *J Biol Chem* 278: 48935 – 48941

Zha J, Weiler S, Oh KJ, Wei MC, Korsmeyer SJ (2000) Posttranslational N-myristoylation of BID as a molecular switch for targeting mitochondrial and apoptosis. *Science* 290: 1761 – 1765

Zhang Z, Zhu W, Lapolla SM, Miao Y, Shao Y, Falcone M, Boreham D, McFarlane N, Ding J, Johnson AE, Zhang XC, Andrews DW, Lin J (2010) Bax forms an oligomer via separate, yet interdependent, surfaces. *J Biol Chem* 285: 17614 – 17627